Reply to the editor (C. Ritz) of tc-2016-167 (Strain localisation and dynamic recrystallisation in the ice-air aggregate: A numerical study. F. Steinbach et al.)

Dear Dr. Ritz,

thank you very much for considering our manuscript for publication in The Cryosphere (IPICS special issue). We considered and addressed the referees' comments, replied to all of them and indicated specific changes that are made in the revised manuscript. The major changes in the revised manuscript are:

1) New discussion sup-chapter "4.5 Limitations of the modelling approach". In particular, the assumption of an incompressible air phase concerned the referees. We regard this an important issue and created a detailed reply that is found at the end of both reply letters.
2) New discussion sub-chapter "4.2 Natural firn microstructures and numerical simulations ", the comparison has moved from section 3. To avoid redundancy, section 2.7.3 has been removed, and is now part of 4.2.
3) Supplementary figures S1 and S2 provide more simulations. The figures are also found with the specific replies.

Two additional changes were (a) the correction of a small error affecting the eigenvalues in Table 2 and Fig. 7, that does not affect the observations and interpretations. (b) After submission, Cyprych et al. published a study that supports our interpretation and adds to the discussion. We added Cyprych et al. (2016) as a reference and refer to the study in the revised manuscript.

The reply letters and a revised manuscript indicating the specific changes were uploaded to the discussion forum, as the following files:

- *AuthorReply_Referee1.pdf*
- *AuthorReply_Referee2.pdf*
- *RevisedManuscript_ChangesHighlighted.pdf*

Thank you very much for your efforts.

With best regards,

Florian Steinbach and co-authors.

Reply to referee comments by Anonymous Referee #1 on TC-2016-167

(Strain localisation and dynamic recrystallisation in the ice-air aggregate: A numerical study. F. Steinbach et al.)

We thank Anonymous Referee #1 for a constructive review and regarding the proposed modelling approach and our conclusions as "sound and (…) reasonable". In the following, we reply to the specific concerns addressed by the referee and state the corresponding changes in the revised manuscript. The referee comments are cited in italics and our reply is in blue font. If not indicated differently, any reference to page or line numbers are with respect to the discussion paper, not the revised version.

General Comments:

This paper presents micro-dynamical simulations of polycrystalline hcp ice containing air bubbles using a numerical approach based on the coupling of the numerical platform Elle, a front-tracking formulation that accounts for microstructure evolution due to different dynamic recrystallization processes (normal grain growth, strain-induced grain boundary migration, recovery, polygonization) and a viscoplastic model based on Fast Fourier Transform (VPFFT) to calculate the micromechanical fields (stress, strainrate, velocity, etc.) due to deformation of the constituent ice crystals by dislocation creep. In particular, the stored energy field calculated with VPFFT provides the driving force for the aforementioned recrystallization processes. Details of the integration between Elle and VPFFT and applications to different geomaterial systems have been reported in previous papers by the same team, including studies of the micro-dynamics of fully-dense ice polycrystals. This paper presents a new application of Elle/VPFFT, to study the ice-air system, aiming at a better understanding of the onset of dynamic recrystallization in, e.g. firn. One of the main conclusions with glaciological relevance of this study is that the presence of air bubbles induces a "composite material" behavior, which contributes to: a) higher strain localization in the ice crystals, and therefore faster onset of dynamic recrystallization compared with fully-dense ice, and b) weaker CPO–not caused by grain-boundary sliding–, as the volume fraction of air increases.

We thank the referee for this concise general comment and summary of the main topics and conclusions of our paper. We are pleased to read that our objectives and conclusions are apparently clearly explained in the manuscript.

Specific Comments:

While the proposed approach is sound and the main conclusions are reasonable, the specific treatment of the air inclusion phase, as far as its constitutive behavior and the treatment of the ice-air interfaces are concerned, needs to be better explained, including a better disclosure of the approximations involved. It is reported (section 2.6) that air bubbles are represented by an incompressible crystalline material with the same crystallography and slip systems as for ice, and that tau_s-air is set 5000 times smaller than tau_basal of ice. This seems to imply (more clarity is needed here) that the air is represented by hcp crystals deforming by basal, prismatic and pyramidal slip with equal critical resolved stresses.

The implications the referee is deducing from our description in section 2.6 are correct. For numerical reasons, air was described as crystalline material (section 2.6, page 8, lines 13-14) with slip systems similar than in ice Ih (basal, prismatic and pyramidal slip). For ice Ih, the pyramidal and prismatic critical resolved shear stresses were 20 times higher than for slip on

the basal plane. The referee correctly assumes that the critical resolved shear stresses for all air slip systems were constant to approximate mechanical isotropy. As outlined in the manuscript, critical resolved shear stresses for the air phase were set 5000 times lower than for ice Ih basal slip. We agree that there is a need to better explain this approximation. Hence, we added a sentence on page 8, line 14. See our following reply for further explanations.

In turn, this implies the somehow unrealistic assumptions of: a) "anisotropic" bubbles (although the anisotropy remains small) and b) a unit cell unable to accommodate any volume change. The first approximation could have been avoided by adopting an isotropic viscoplastic behavior, or, even better, imposing zero stiffness (i.e. vanishing stress) to the unodes belonging to the air phase. With this said, I suspect (but I'd like to hear this from the authors!) that the predictions would not be dramatically affected.

We agree with the referee: Admittedly, this approach does not allow for a fully isotropic air material as deformation is only possible on defined slip systems. Our simplified approximation of the description of air inclusions is only correct if the results would not be dramatically affected by the unrealistic assumptions the referee was mentioning. Therefore, we updated our VPFFT code to impose zero stiffness to unodes in air inclusions (as suggested by the referee) to assume an air phase independent of any crystallography. For this comparison, the initial setups of F20 were used and deformed in one increment of pure shear to 1% vertical shortening to obtain instantaneous strain rates and stresses. We compared the results of the updated approach ("zero stiffness") with the VPFFT version used for the simulations presented in the manuscript (see attached figure R1.1). The results show:

(1) No significant difference in normalised von Mises strain rates, i.e. the location and intensity of strain localisation (cf. localisation factors "F")

(2) No significant difference in von Mises stresses for each unode obtained from the VPFFT output

(3) When using the VPFFT approach used for the simulations in the manuscript, mean pressure of both ice and air phase are zero. The variation in pressure in the air phase is very small and between one and two orders of magnitude smaller than in the ice phase.

One of the main observations of our study is that air inclusions cause and intensify strain localisation which provides driving forces for dynamic recrystallisation. The results of our comparison presented in figure R1.1 therefore indicate, that our treatment of the air phase as a very soft quasi-isotropic ice Ih crystal does not affect the predictions of the simulations. Using 5000 times softer slip for air "slip systems" than for ice basal slip and a stress exponent $n = 3$, we assume an even higher effective viscosity difference between the materials, which underlines why the results presented in figure R1.1 are essentially the same. As the results are almost identical, we did not re-run the simulations presented in the manuscript, but future simulations should use the new and updated VPFFT approach. Figure R1.1 will be provided as supplementary material.

In order to better discuss and present approximations made for the simulations (also the ones mentioned by referee #2), we added a paragraph to the new sub-chapter discussing model simplifications (4.5 Limitations of the modelling approach), where the simplified treatment of the air phase is discussed. We mention that for reasons outlined above our treatment of the air phase does not significantly affect the results.

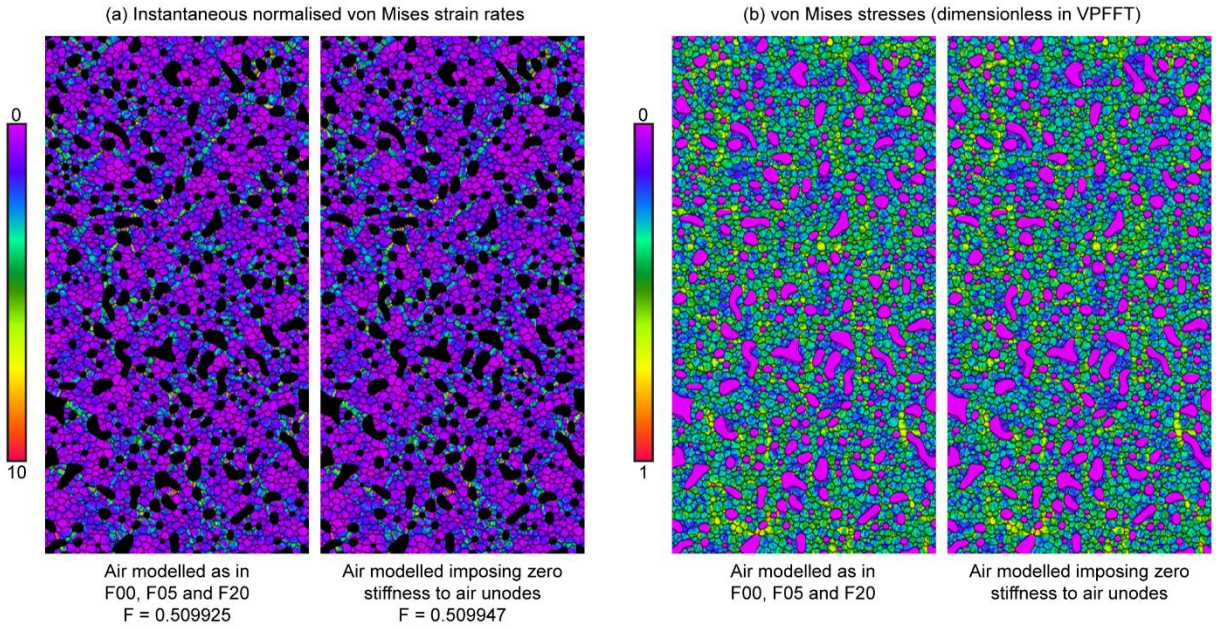

Figure R1.1: Comparison of the VPFFT model used for the simulations presented in the discussion paper with an modified algorithm that imposes zero stiffness to air unodes. These simulations comprised one step of VPFFT with an increment of 1% vertical shortening using the same initial setup as for simulation F20. We provide this figure as supplementary material and refer to it in the revised manuscript.

The second approximation is more delicate. The air phase/unit cell incompressibility implies the inability of the present approach to consider volume changes that are inherent to ice flowing under its own weight. Moreover, the incorporation of a constitutive description admitting compressibility would have also allowed improving the convoluted treatment of the behavior of the ice-air interfaces described in section 2.4.1, accounting explicitly for the effect of the bubbles' internal pressure, both in terms of mechanical behavior and as a controlling factor of the recrystallization process. Furthermore, the shortcomings associated with the simplified treatment of the air bubbles as an incompressible phase may be responsible for the somehow puzzling results, in the cases of the F05 and F20 microstructures, showing the overall porosity almost unaltered after ~50% vertical shortening. This makes the comparison with the EDML ice core at 80m depth presented in Fig. 8 questionable. This needs to be acknowledged and further model improvements to mitigate these limitations be discussed, before this paper is accepted for publication in The Cryosphere.

We thank the referee for pointing out an important assumption made in our simulation approach. Also referee #2 commented on the assumption that air is modelled as an incompressible material. In consequence, no porosity changes are possible during our simulations. The referees' concerns are clearly justified and correct. In the following we aim to better explain why we chose to use this assumption and discuss possibilities to mitigate this limitation. This reply can also be found at end of the reply to referee #2.

By imposing pure shear, we assume a deformation mode that conserves the total area of the simulation box, which does theoretically not allow for any volume change and implies conservation of mass for both phases. However, firn is characterized by most vertical shortening achieved by compaction of the pore space causing a significant air volume loss. In general, we would like to remark, that the evolution of our numerical microstructures cannot be regarded as an evolution with depth (as would be the case in natural firn and ice). In fact, the microstructure in each simulation step can be regarded as the microstructure that results from the deformation of a material with an unknown previous porosity to the actual situation. We refrain from any study of depth evolution of porosity, inclusion shape or distribution and

remark, that the scope of the manuscript is a study of deformation and recrystallisation processes within the ice at the presence of a very weak phase.

Theoretically, the compaction of a pore is a function of the surface energy driving inward bubble surface movement and the inner bubble pressure counter-acting this movement. The latter depends on parameters such as the overburden pressure, bubble shape and connectivity. In a state of equilibrium, a bubble's size is does not change implying static conditions. Since the simulations do not incorporate gravitational forces, overburden pressure is unknown and the theoretical "area energy" is used to counter act surface energy (cf. section 2.4.1, equations (3) and (4) and Roessiger et al., 2014). The pre-factor c can be regarded as an approximation of a compressibility factor that controls how quickly this equilibrium is reached (Roessiger et al., 2014). The lower the factor c, the less "area energy" is counter acting the surface energy that tends to decrease the overall cross sectional area of the bubbles. In turn, this means more cross sectional area change is allowed causing a stronger violation of the conservation of mass requirement.

To fulfil the conservation of mass requirement in our simulations, any movement of the ice-air interface that is not mass conserving should actually be inhibited. This would however lead to complete "freezing" of the interfaces, an even more unrealistic assumption. Therefore, we allow movements of the ice-air interfaces that preserve the overall porosity, but still allow for sufficient shape changes of the bubbles. Preparatory tests yielded $c = 0.1$ as a compromise to achieve this. With this, we use a 10 times higher factor c than Roessiger et al. (2014), who modelled static conditions without deformation.

The current VPFFT code does, unfortunately, not include a compressible phase or voids. This is not an intrinsic limitation of the model, and a version without this limitation is under development. The current model is, therefore, not capable of simulating compaction, and we limited ourselves to area-conservative pure shear. Admittedly, this raises questions on the comparison of the simulations with the EDML firn image (Fig. 8). In the revised manuscript, we discuss the limitations associated with assuming incompressibility and explicitly highlight, that the comparison with the firn image has to be taken qualitatively and as a comparison of inferred processes and their expression in the microstructure.

Specific actions taken in the revised manuscript:

1. As a reaction to both referees' concerns, we created the new sub-chapter "4.5 Limitations of the modelling approach" to discuss approximations made in our simulations. A condensed version of the explanations above is part of this chapter.
2. The role of the pre-factor c and our choice of $c = 0.1$ is now better explained in section 2.4.1 and in the new section 4.5.
3. The comparison with the EDML firn image (Fig. 8) has moved to another new sub-chapter in discussion (section 4.2). We present the natural firn image as a first qualitative comparison with an Elle/VPFFT simulation on ice microdynamics. The intention of this comparison is trying to identify processes observed in the simulations also in natural firn (i.e. strain localisation in the vicinity of bubbles associated with enhanced dynamic recrystallisation). The limitations caused by the modelling approach are discussed and we state that we refrain from any quantitative comparison.

Reply to referee comments by Anonymous Referee #2 on TC-2016-167

(Strain localisation and dynamic recrystallisation in the ice-air aggregate: A numerical study. F. Steinbach et al.)

We are thankful for the useful und constructive review of referee #2 in which our paper is regarded as "well written" and the analysis as "valuable". In the following, we reply to the specific concerns addressed by the referee and state the corresponding changes in the revised manuscript. The referee comments are cited in italics and our reply is in blue font. If not indicated differently, any reference to page or line numbers are with respect to the discussion paper, not the revised version.

Full-field numerical analysis of high density cold firn.

This paper aims to study the competing processes of normal grain growth, polygonization, and migration recrystallization in cold firn (very close to the density of ice). Their 2D model shows the importance of strain localization triggered by air inclusions that gives rise to locally high strain energies that drive grain boundary migration.

Overall, this paper is well written and I think this is a valuable analysis and the expressions of strain localization apparent in the model show that there is much more heterogeneity in recrystallization process in ice than we usually assume.

My primary concern with this paper is that some of the assumptions make it difficult, at best, to compare to the EDML firn thin sections. That does not say that the simulations aren't valuable, I just think the authors need to be upfront and clear from the beginning what the simplifying assumptions are and how that affects their comparison. They state in the last sentence of the discussion that the comparison should be taken only approximately, but up until then they give the impression that they believe it is a very valid comparison.

We are thankful for that helpful advice. Referee #1 raised similar concerns and we therefore decided for some general changes in the manuscript (details are outlined within the replies). In the following we summarize these changes and give some general comments:

(1) The comparison between an EDML firn core image and simulation results has moved in a new sub-section in discussion (new section "4.2 Natural firn microstructures and numerical simulations" in revised manuscript). To avoid redundancy, section 2.7.3 was removed, and the condensed content is found in the new section 4.2. The comparison intends to provide a first comparison of an Elle/VPFFT model of ice micro-dynamics to natural samples. The comparison is designed as a purely visual and qualitative comparison that compares processes observed in the simulation and suspected in natural firn (namely the process of strain localisation in the vicinity of bubbles and the related increased strain energies driving dynamic recrystallisation).

(2) We created another new sub-section in discussion in the revised manuscript ("4.5 Limitations of the modelling approach"). Here, we discuss in more detail the approximations and limitations of the approach and discuss possible solutions for future studies.

In particular:

1. 2D versus 3D

Correct, the stereological effect when comparing 2D models with 2D slices from a 3D sample is important. A theoretical circular grain (or bubble) in our simulations can be imagined to continue as an infinite cylinder in the 3rd dimension. Hence, any cross sectional area in a 2D plane cut parallel to the modelling plane will be the maximum cross sectional area possible. This is the major difference between our 2D simulations and a 2D cut through a 3D sample of natural ice. In a natural 2D sample, the cross sectional area of a grain is to a certain probability not the maximum cross sectional area of this grain (e.g. see the work of Anderson et al. (1989) in Philosophical Magazine B). Essentially this means that our simulations exhibit the maximum grain areas possible, however, a 2D cut through a 3D natural sample tends to underestimate the real grain sizes. In order to do a proper grain size comparison between simulation and natural sample (but we refrain from doing this), corrections on the natural 2D grain size would be necessary.

The abovementioned is summarized in the new sub-section in discussion (4.2 in revised manuscript) that compares the EDML firn image with modelling results.

2. The size and distribution of air pockets is set for each run but no information is given as to why those values were chosen. I would expect more smaller air pocket to behave differently than fewer larger air pockets, even with the same percentage of air. And visually, it looked like too few air pockets (although perhaps they assume the ice has undergone significant grain growth before reaching their initial microstructure).

The distribution of air inclusions was designed by using an initial setup of pure ice and setting air properties to random ice grains. We hoped this to cause the most realistic bubble distribution. The number of grains was chosen to later (after applying surface energy boundary migration) produce the desired fractions of air (0, 5, 20%). Afterwards, surface energy based grain boundary migration was applied causing the air bubbles to adopt more realistic (circular) shapes. It is correct, that there is a lower number of air inclusions in the simulation image than in the presented EDML firn image. We can expect that the size and distribution of air inclusions does not significantly change the processes interpreted from the results (localisation and locally high strain energies). Some more comments on this:

- The main effect of the absolute size of the bubbles is on their ability to maintain a circular shape. Small bubbles are more rounded than large ones in the model (see figure R2.1) and predicted by theory (discussed, for example, in Walte et al. 2011. Earth and Planetary Science Letters 305, 124-134). The shape of the bubbles is comparable to those observed in firn and bubbly ice.
- The size of bubbles relative to that of ice grains is possibly more important than the absolute size of bubbles. This determines the fraction of grain boundaries influenced by nearby bubbles and those further away (Roessiger et al. 2014. Journal of Structural geology 61, 123-132). A systematic study of this effect was not undertaken here, as the work focussed on the localisation behaviour induced by the presence of bubbles.
- The strain localising effect of air inclusions giving rise to locally higher strain energies driving dynamic recrystallisation is hardly affected by the size and distribution of bubbles: We did systematic tests on how the distribution of bubbles affects this general observations in the manuscript (see figure R2.1). The tests are comprised of two simulation setups, one with many small inclusions, another one with a low amount of large inclusions. The overall fraction of air is constant in both setups and the same as in setup F20. The results show that strain localisation in the sense as described in the manuscript is still occurring with many small and a few large air inclusions.

We added figure R2.1 as a supplementary figure (S1) showing the results of the mentioned trial simulations. Furthermore, we acknowledge that comparing size, shape and distribution of bubbles with natural samples is not possible and not our aim.

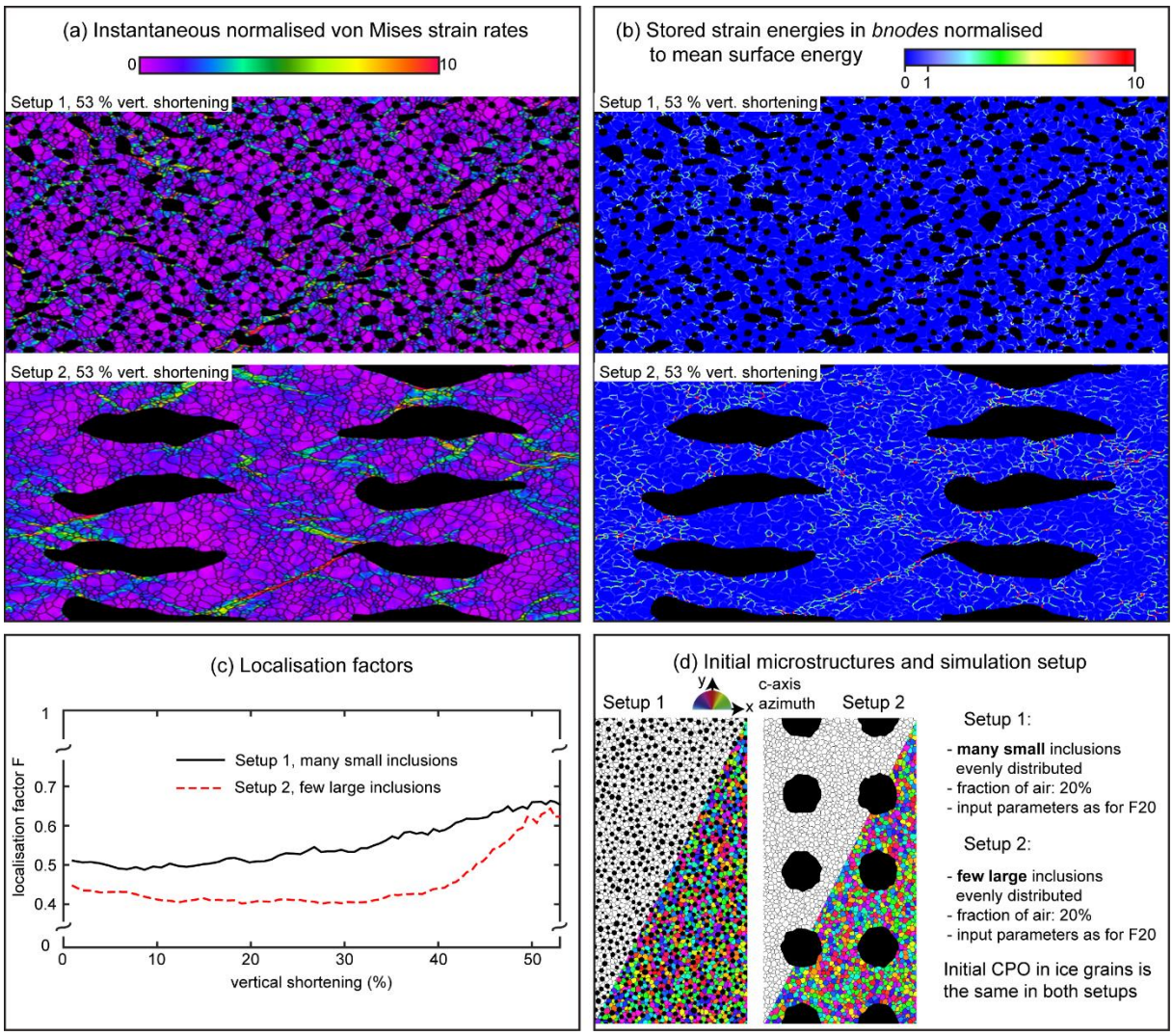

Figure R2.1: Comparison of simulations varying the distribution of air inclusions. The simulations were performed under the same conditions as for simulation F20, which is presented in the manuscript. The results show that strain localisation and associated locally higher strain energies are occurring in both setups. A notable difference is that large bubbles cannot maintain their approximately circular shape. We provide this figure as a supplementary figure and refer to it in the revised manuscript.

3. The model air in the mixture is incompressible (yet, in real firn, it is highly compressible).

We agree with the referee; this is an important point that needs more clarification as it has also been mentioned by referee #1. Since we regard this clarification as important, we created a detailed reply that is found at the end of this document. Please find more explanations in this section.

4. The stress regime is designed to generate 50% compressive strain along the vertical axis, this is accommodated by extension laterally (i.e. pure shear). The firn at EDML may have undergone 50% compressive strain along the vertical axis, but this was accommodated by densification including compression of air pockets (i.e. uniaxial compression). These are two very different stress regimes.

The stress regimes in simulation and firn are indeed very different. We are unfortunately currently not able to model a stress regime more similar to the one observed in firn. Our assumption of assuming an incompressible air phase relates to this deformation mode that is not allowing for area changes (see specific reply at the end of this document). In the revised manuscript, we discuss this point when comparing to EDML firn (section 4.2).

5. The grain size is HUGE compared to real polar plateau firn. This is not really discussed until the very end of the discussion. I had a difficult time figuring out why they started with such large crystals. Similarly the increments of 1% strain are high, how does this large crystals with fast strain rates affect the solution - does this prevent recovery from acting?

Admittedly, the chosen initial and resulting final grain size is large in comparison to natural firn grain sizes. Visually, the natural firn image and simulation result are comparable, however, the actual grain size of the model is about an order of magnitude higher and the strain rate is faster (cf. 2D/3D effects outlined before).

We decided for this large initial grain sizes mainly to make our simulations comparable to the ice simulations without air bubbles by Llorens et al. (2016a,b). Preparatory sensitivity tests showed that final grain sizes strongly vary with parameters such as mainly mobilities, critical high angle grain boundary angle for polygonisation or energy per dislocation line. We chose to use literature values for these parameters to allow comparability with previous modelling instead of introducing new values for these parameters. Unfortunately, with these given input parameters, the simulations predict larger grain sizes than expected from firn and the fast input strain rate. We would like to remark, that although rigorous experimental studies have been performed to determine some of the material properties (e.g. by Nasello et al. (2005) on mobilities), we cannot be sure of how applicable those are for numerical models. Presumably, especially the numerical mobilities need proper adjustment to quantitatively compare future simulations to natural microstructures. Furthermore, the effect of micro- to nanoparticles is suspected to decrease boundary migration and hence boundary migration rates, but is currently not incorporated in the numerical approach. The discrepancy in grain size actually shows that the modelling can be used to gain better estimates of often poorly constrained values of a range of parameters, such as grain-boundary mobility, dislocation energy, etc. This was, however, not the aim of this study.

About the “high” increments of 1% strain together with large crystals and strain rate: This increment is actually the lowest one so far used in this kind of models on ice microdynamics. Simulations by Llorens et al. (2016a,b) and Jansen et al. (2016) use increments at least twice as high. Lower increments lead to error reduction, but increase computation time. Currently increments of 1% provide the best compromise between both. Future code refinements aim to allow smaller increments. Recovery is not prevented from acting, but still occurring associated with polygonisation, which is visible in the simulation videos (supplementary material).

We remark that large grain sizes only affect the Elle based recrystallisation approach. The VPFFT approach is dimensionless and is only affected by a lower resolution limit, which is determined by the number of *unodes* in the simulation. As strain localisation is caused by the distribution of viscoplastic deformation provided by the VPFFT code, we cannot expect a strong effect of grain size controlling strain localisation and the balance of driving forces for static and dynamic recrystallisation. In fact, as VPFFT is dimensionless and still provides strain localisation bands in any kind of setup, future research should investigate if strain localisation in ice is a scale independent process.

In the new sub-chapter 4.2, we acknowledge that our grain sizes are only qualitatively comparable with natural firn. We also added a discussion of the numerically predicted grain sizes to the new sub-chapter “4.5 Limitations of the modelling approach”.

The overall conclusions of the model as it is presented are still valid. I would prefer to see the following changes:

1. Better explaining the effects of assumptions 1-5 above on the comparison between model and real firn.

We created a new sub-chapter in discussion (4.2) to compare to EDML firn and include a discussion of these assumptions.

2. Either provide additional models that show better how the size of air pockets affects the results or at the very least, discuss the effect of this assumption on the results.

We performed trial simulations to test how the size and distribution affects the results and, more specifically, the conclusions drawn (see figure R2.1). The total fraction of air in these tests is constant and the same as in setup F20 (like the remaining input parameters). While the 1st setup has a high number of small bubbles, the 2nd setup has a low number of large bubbles. Strain localisation between the air inclusion that produces locally high strain energies driving dynamic recrystallisation is observed in all these simulations.

We now provide figure R2.1 as a supplementary figure (S1) and mention it in the revised manuscript.

3. Either provide additional models that allow for some compression of the air, which might minimize some of the strain localization if deformation of the air can accommodate the changes needed in the ice crystals. Or, minimally, discuss the effects of this assumption on the solution.

Unfortunately, the current numerical setup is not able to correctly include the effect of compaction, please find more explanations on this topic in a detailed reply at the end of this document. We agree that the effects of our assumption at least need to be discussed in more detail. This discussion and an explanation of ways to mitigate this limitation in future studies is part of the new sub-chapter "4.5 Limitations of the modelling approach".

Specific Comments:

Abstract: P1 Line 9/10: The first two sentences seem redundant.

We understand the redundancy the referee sees in this expression and are thankful for this hint. For clarification: The first sentence was intended to briefly introduce what we did. With the second sentence we wanted to highlight that we are the first to present and use such a modelling approach for dynamic recrystallisation and deformation in ANY polyphase crystalline aggregate (including rocks, metals, etc.). To avoid any redundancy and use a more precise expression, we changed the second sentence of the abstract.

Introduction P2 Line 1: "very" doesn't add anything

We agree. The word "very" has been removed.

Line 13 and 16 - I am puzzled by some citations, Treverrow did not discover that CPO causes anisotropy, Montagnat was not the first to describe the effect on flow. While these are good papers, please cite papers that added to the discussion (and tell me why they added). These papers probably should be cited, but there are many more that have also contributed specific new ideas to the discussion, so please be specific as to why you have chosen those papers.

We thank the referee for this hint.

We chose to use to cite this literature on CPO causing mechanical anisotropy since Budd and Jacka provided an overview in their review paper and Treverrow et al. is a more recent work supporting that CPO causes anisotropy. Montagnat et al. (2011) was used as a more recent study that (a) explicitly mentions that recrystallisation influences the flow of ice (b) using two both numerical modelling and experimentally deformed ice. However, we see that we should choose

more suitable literature here and be specific about what we want to express. Out specific changes are:

- We now also refer to the early experimental work by Steinemann (1954) and Gao and Jacka (1987) and explain that these studies contributed to our knowledge about CPO causing large-scale mechanical anisotropy.
- We omitted the reference to Montagnat et al. (2011). We want to highlight that recrystallisation affects fabric developments, which is in turn affecting the creep behaviour. We therefore now cite three papers that contributed to how rotation recrystallisation and (static and dynamic) grain boundary migration affect fabric development and hence the creep behaviour (Duval and Castelnau, 1995; Castelnau et al., 1996; Duval et al. 2000). We changed the sentence on page 2 line 15.

There is a similar issue on page 3, Lines 29 and 30 - These two papers were not the first to describe folding in ice sheets due to anisotropy.

The referee is correct. Those two papers are not the first to describe folding in relation to anisotropy. However, this is not what we intended to express in this sentence: In fact, the whole paragraph is intended to give the reader a brief overview on the Elle platform and how it has been applied in similar studies (cf. beginning of the sentence: "Recent applications of methods (…) are (…)."). We chose to cite these two papers at this point because they represent the first application of Elle / VPFFT on the topic of folding in ice sheets. With respect to this intention of the paragraph, the citations should be suitable and valid.

We are still thankful to the referee for pointing out this issue, apparently we need to make more clear why we chose to use these citations. As a reaction, we changed the beginning of the sentence (page 3 line 27) to be more clear about the intention of this sentence.

P3 Line 9: operate - present tense (please check all tenses).

Thank you, we changed this. All tenses have been double checked.

P4 Line 28: accommodated

Thank you for the hint. We changed this.

P6 Line 1 – redundant

We agree with the referee. The sentence on page 5 line 26-27 already mentioned that the stored strain energy was not taken into account for ice-air boundaries. We changed the sentence on page 6 line 1 accordingly.

Line 8 - How did you determine c and Mo and several of the parameters? I'm not sure I saw much in the way of a sensitivity study on the effect of variations in the parameters.

Most parameters were chosen according to published literature (wherever a reference is given). Numerous sensitivity tests took place during the development of the model. In summary, they show how sensitive the model is to changes in mainly the grain boundary mobility or other parameters such as the assumed high angle grain boundary angle. Hence, most of the parameters were set to the values of either previous numerical modelling (to allow comparability), experimental work or other literature values. We did not want to introduce new values differing from previous studies as this would require more detailed sensitivity tests, which is beyond the scope of the paper. In addition, we chose literature values as they mostly resulted in low numerical errors and hence a stable simulation.

An example for a parameter that is not given by the literature is the factor c (section 2.4.1). We chose to assume equilibrium between surface energies shrinking the bubbles and inner bubble pressures counter-acting the shrinkage. In turn, this causes our simulations to assume

incompressibility for the modelled box (please find more information in our detailed replyon the incompressibility assumption and in new sub-chapter 4.5). To achieve this equilibrium during the simulations, preparatory tests yield that c=0.1 is a good compromise that still allows the bubbles to maintain a realistic (circular) shape, without causing unacceptable changes in air fraction.

In the revised manuscript, we now better explain why we use c = 0.1 after the paragraph ending on page 6 line 14 (in discussion paper). On page 7 line 18 of the discussion paper (α_{hagb} = 5 °), we added a half sentence to express that we used this critical angle to be conservative. A smaller angle would lead to lower grain sizes as grain splitting by polygonisation is the most effective grain size reducing mechanism in our simulations. We expect that this would cause dynamic recrystallisation to become even more obvious as more small grains along high strain zones would develop.

Line 15 - I think you can explain this a little more. Provide a little information as to why you selected those values - more than just the citation, so we don't have to go read the other papers.

This relates to the previous comment. We changed this paragraph to provide more information about the mentioned parameters in this paragraph. For further explanation, see our reply to the previous comment.

Lind 30 - "Recover be" ?? perhaps "by"

Thanks, that has been changed

P7 Line 30 - "on" the results

Thanks again, we changed it.

P8 Line 2 - why was 0,5, and 20 chosen, especially considering that 10% is a commonly assumed volume of air for the bubble close-off depth?

The referee is correct: 10% porosity is usually assumed for the firn-ice transition. Our goal was not to investigate processes at the firn-ice transition only, but in a theoretical ice-air aggregate in general. For this reason, we chose three different porosities, 20% for the material in firn (above the firn-ice transition), 5% for bubbly ice well below the firn ice transition and 0% for comparison and reference. Additionally, our simplification of assuming an incompressible air phase does not allow us to relate our simulation to any specific depth (or porosity) in the ice or firn column, which is why we refrained from using "real firn" porosities.

We agree that this intention should become clearer in the manuscript and added three sentences on page 8 line 3.

Line 8 - repeated value for c, but still no explanation for that value.

There is obviously a need for us to be more specific here: This sentence explains how we introduced the air inclusions in the numerical microstructure. To create initial setups for F05 and F20, air conditions were set to a number of grains in setup F00 followed by applying surface energy based boundary migration, which allowed them to adopt a near 180° dihedral angle (i.e. a circular shape). For this purpose, we also needed to decide for a factor c and for consistency used the same value as for the actual dynamic recrystallisation and deformation simulations. This is what we wished to express here. Pleased find a description on why we chose for $c = 0.1$ in the specific reply on incompressibility assumption that is provided at the end of this document.

To avoid that our expression can misleadingly be understood as a repetition, we changed the last sentences of this paragraph. An explanation why c = 0.1 was used is added (cf. our corresponding reply at the end of this document).

P10 Line 13 - I realize that I haven't look at firn microstructure as much as Sep Kipfstuhl, but I was not under the impression that air pockets coalescing was a commonly occurring process in polar firn. I typically think of the pockets compressing and getting pushed to trip junctions, but not coalescing.

On page 10 line 13, we did not want to express that bubbles coalesce as would be expected in firn, but instead we intended to state a basic observation on the simulations. Coalescence in simulations would be expected from simulations on static grain boundary migration in the ice-air aggregate by Roessiger et al. (2014). Evidently, we see that the large air inclusions in the simulations are created due to coalescence (see supplementary movies). Therefore, mentioning this basic observation in results section is correct.

Coalescence of bubbles is a function of deformation and surface-energy effects. It is observed in experiments on liquid (melt) pockets in deforming rocks and happens in the simulations. If the bubbles shrink faster than the convergence caused by deformation, coalescence would be suppressed. This may be the case in natural firn, but is difficult to ascertain. Due to the high surface energy, a new bubble that results from a merger very quickly regains a spherical shape. Bubble coalescence is therefore difficult to determine from bubble shapes only. Bubble size distributions may be a better (or only?) way to determine the importance of coalescence in natural samples (Roessiger et al. 2014).

We did *not* change the sentence on page 10 line 12, because the basic observation of coalescing "numerical bubbles" is correct (see supplementary video). Since this is the results section, any discussion on this topic would be inappropriate. But: We added a remark in the new sub-chapter 4.2 (comparison with EDML sample) that bubble coalescence may be less common in natural firn than in our simulations.

P11 Line 30 - "Apart from the scale difference… " This is where I have issue with the comparison. This very qualitative comparison for two very different systems seems strange (yes apples and oranges are both round and about the same size, so do we assume they are the same?). I don't argue that there are likely some of the same processes going on, I just don't think the comparison is done in a rigorous enough way. If the authors want to maintain this subjective comparison, it might be best shifted to the discussion section, than the results section, even better in a special part of the discussion section, so that it is clear that a direct rigorous comparison is not possible because of the assumptions, but it is still valuable to visually look. That kind of comparison does NOT belong in the results section.

We agree with the referee's concerns. As outlined by the referee, we wanted the comparison to be qualitative and purely visual. It intends to compare the processes going on and show, that both in simulation and (probably) in natural firn, strain localisation as a result of bubbles as a second phase occurs and leads to locally higher strain energies associated with dynamic recrystallisation.

As described in other parts of the results, we moved the comparison to a new sub-chapter in discussion (4.2 in revised manuscript). We state that the comparison is qualitative and discuss the assumptions made for the simulation. In the course of this, we moved and shortened the explanations of methods section 2.7.3 to the new sub-chapter. Furthermore, we avoid the expression "apart from the scale difference (…)".

P13 Line 15-20 - I had always understood that dynamic recrystallization was possible everywhere given strain energies, but is a much more dominant process above -10 (an activation energy transition point). Line 30 - "the initiation of this process is not only temperature dependent" - I'm not sure that anyone ever said that it's "initiation" was "only" temp dependent? In larger scale modeling is it much easier to parameterize the migration recruits as being temp dependent, but this is a parametrization commonly used. Because the

authors don't provide any comparison models, it is hard to tell how "dominant" the process is in -30 firn versus -10 firn. My main concern here is that they state that strain rate controls dynamic recrystallization as if that were a new idea. This last statement would be more compelling if they presented a sweet of models at different temperature and different stress regimes both with and without the dynamic recrystallization process - to be able to show the effects of this process being active or not. Without any comparison simulations, it is hard to show what the effects are.

The referee is correct that no one ever strictly said that the initiation of strain induced boundary migration is only temperature dependant. However, it has been proposed in earlier studies that "migration recrystallisation occurs for temperatures higher than -10°C" (Duval and Castelnau, 1995). This we interpret as that it is *most dominant* at temperatures of -10°C or higher. Our modelling, together with previous observations on firn by e.g. Kipfstuhl et al. (2009) or Faria et al. (2014b, Appendix B), shows that even at lower temperatures the strain energies can drive dynamic recrystallisation and that, therefore, strain induced boundary migration can be a significant or even dominant processes.

We thank the referee for pointing out this inaccurate expression. We changed the sentence at page 13 lines 15-17 and page 13 lines 29-31 to use similar expressions to those in our reply above and outline that Duval and Castelnau (1995) suggested that strain induced boundary migration is *most dominant* at temperatures of -10°C or higher.

P14 Line 5-8 - this discussion about experimental strain rate and grain size selection should be up in methods (or maybe results), not in the discussion.

Thank you for pointing this out. The statement on grain sizes has moved to section 2.6 (Methods: Simulation setup) mentioning that we used these grain sizes to be consistent with Llorens et al, (2016a,b). The statements on strain rates were actually redundant on page 14, lines 6-9, which is why we merged them and moved the statement to section 2.6. Effectively, this means we removed the contents on page 15 lines 3-11 (see reply to following comment).

Line 10 - this should be in the methods section

We agree. The paragraph has been condensed into three sentences and moved to the methods section 2.6.

Line 19 - specify what "it" is to be clear here

Thanks, this expression needs improvement. Llorens et al. (2016b) show that with recrystallisation active, it is difficult or impossible to see the actual strain distribution or strain localisation in the grain boundary network. Strong recrystallisation rapidly overprints any strained grain boundary, which makes the grain boundaries unsuitable as strain markers. The actual strain heterogeneity in ice is therefore higher than the boundary network may suggest.

What we mean here with "it" is strain localisation. We changed the sentence accordingly.

Line 25 - awkward sentence structure, please rewrite.

Thank you, we rewrote the sentence structure in the revised manuscript.

Line 33 - less, not lower

Thanks, we changed it.

P 15 Line 14-15 - this statement should be early on in manuscript, or at least at the beginning of a discussion section about the comparision, not as an afterthought.

We agree with the referee that this statement is important and underlines that the results have to be discussed with respect to the model approximations. We shifted this sentence in front of the discussion chapter on grain size analyses and accordingly changed the first paragraph. As

the comparison with the EDML firn image moved to the discussion, we also highlight the statement in the new sub-chapter 4.2. Furthermore, the new sub-chapter on limitations of the modelling approach (4.5) should clarify this even more.

Line 17-25 - A conclusion should be used to talk about the these results in the context of larger questions. This is rather short conclusion that just repeats what has already been said. Please add some kind of bigger picture context. Why is it important to recognize that migration recrystallization happens (although slowly) in the firn? What can we do with this information in the future?

We are thankful for this suggestion and took the opportunity to modify the conclusions by adding:

- Ice sheet deformation may be more heterogeneous than previously thought.
- Strain localisation is not the exception, but rather the rule in ice sheets and glaciers. Together with anisotropy, second phases (such as air bubbles) provide an effective mechanism for strain localisation.
- Localisation is a process that could be considered in future firn densification models
- Due to strain localisation, the rate of fabric change is locally higher. This may happen especially in firn, where bubbles are most abundant and can cause localisation.
- The used VPFFT code is dimensionless, future research could focus on the question whether strain localisation may generally occur on a range of scales in ice.

Table 1 - There is no discussion of the sensitivity of the model results to the selected parameters. Please provide some information.

The referee's comments on page 6 lines 8 and 15 expressed similar concerns, we kindly ask the referee and the reader to find our more detailed reply after these comments.

We agree with the referee, that this needs more clarification and we therefore changed the text in the corresponding parts in section 2 (see our specific reply to referee's comments on page 6 line 8 and 15) to contain more information on the selected parameters.

We now also refer the reader to section 2.4 and 2.6 in the table caption.

Table 2 - just to reiterate when I saw this table, I was shocked at how large the grains were, the discussion of grain size is buried deeply in the discussion, please bring it up front.

We agree with the referee, that the discussion of the large grain sizes needs more clarification, especially when it comes to a comparison with EDML firn images. As mentioned before, we moved this comparison to the discussion section (new sub-chapter 4.2) and discuss with respect to the numerical grain sizes. Please find more explanations in our reply earlier in this document on the general comments on assumptions made in the modelling approach (in particular assumption 5).

Figure 1 - I like this figure!

Figure 2 - I also like this figure, nice job explaining the components of the model.

We are glad about these kind of remarks.

Following page: See our reply to the referee's comment on our assumption of an incompressible air phase.

Reply on referee's comments on assuming an incompressible air phase

We thank the referee for pointing out an important assumption made in our simulation approach. Also referee #1 commented on the assumption that air is modelled as an incompressible material. In consequence, no porosity changes are possible during our simulations. The referees' concerns are clearly justified and correct. In the following we aim to better explain why we chose to use this assumption and discuss possibilities to mitigate this limitation. This reply can also be found at end of the reply to referee #1.

By imposing pure shear, we assume a deformation mode that conserves the total area of the simulation box, which does theoretically not allow for any volume change and implies conservation of mass for both phases. However, firn is characterized by most vertical shortening achieved by compaction of the pore space causing a significant air volume loss. In general, we would like to remark, that the evolution of our numerical microstructures cannot be regarded as an evolution with depth (as would be the case in natural firn and ice). In fact, the microstructure in each simulation step can be regarded as the microstructure that results from the deformation of a material with an unknown previous porosity to the actual situation. We refrain from any study of depth evolution of porosity, inclusion shape or distribution and remark, that the scope of the manuscript is a study of deformation and recrystallisation processes within the ice at the presence of a very weak phase.

Theoretically, the compaction of a pore is a function of the surface energy driving inward bubble surface movement and the inner bubble pressure counter-acting this movement. The latter depends on parameters such as the overburden pressure, bubble shape and connectivity. In a state of equilibrium, a bubble's size is does not change implying static conditions. Since the simulations do not incorporate gravitational forces, overburden pressure is unknown and the theoretical "area energy" is used to counter act surface energy (cf. section 2.4.1, equations (3) and (4) and Roessiger et al., 2014). The pre-factor c can be regarded as an approximation of a compressibility factor that controls how quickly this equilibrium is reached (Roessiger et al., 2014). The lower the factor c, the less "area energy" is counter acting the surface energy that tends to decrease the overall cross sectional area of the bubbles. In turn, this means more cross sectional area change is allowed causing a stronger violation of the conservation of mass requirement.

To fulfil the conservation of mass requirement in our simulations, any movement of the ice-air interface that is not mass conserving should actually be inhibited. This would however lead to complete "freezing" of the interfaces, an even more unrealistic assumption. Therefore, we allow movements of the ice-air interfaces that preserve the overall porosity, but still allow for sufficient shape changes of the bubbles. Preparatory tests yielded $c = 0.1$ as a compromise to achieve this. With this, we use a 10 times higher factor c than Roessiger et al. (2014), who modelled static conditions without deformation.

The current VPFFT code does, unfortunately, not include a compressible phase or voids. This is not an intrinsic limitation of the model, and a version without this limitation is under development. The current model is, therefore, not capable of simulating compaction, and we limited ourselves to area-conservative pure shear. Admittedly, this raises questions on the comparison of the simulations with the EDML firn image (Fig. 8). In the revised manuscript, we discuss the limitations associated with assuming incompressibility and explicitly highlight, that the comparison with the firn image has to be taken qualitatively and as a comparison of inferred processes and their expression in the microstructure.

Specific actions taken in the revised manuscript:

1. As a reaction to both referees' concerns, we created the new sub-chapter "4.5 Limitations of the modelling approach" to discuss approximations made in our simulations. A condensed version of the explanations above is part of this chapter.
2. The role of the pre-factor c and our choice of $c = 0.1$ is now better explained in section 2.4.1 and in the new section 4.5.
3. The comparison with the EDML firn image (Fig. 8) has moved to another new sub-chapter in discussion (section 4.2). We present the natural firn image as a first qualitative comparison with an Elle/VPFFT simulation on ice microdynamics. The intention of this comparison is trying to identify processes observed in the simulations also in natural firn (i.e. strain localisation in the vicinity of bubbles associated with enhanced dynamic recrystallisation). The limitations caused by the modelling approach are discussed and we state that we refrain from any quantitative comparison.

Strain localisation and dynamic recrystallisation in the ice-air aggregate: A numerical study

Florian Steinbach[1,2], Paul D. Bons[1], Albert Griera[3], Daniela Jansen[2], Maria-Gema Llorens[1], Jens Roessiger[1], Ilka Weikusat[1,2]

[1]Department of Geosciences, Eberhard Karls University Tübingen, 72074 Tübingen, Germany
[2]Alfred Wegener Institute Helmholtz Centre for Polar and Marine Research, 27568 Bremerhaven, Germany
[3]Departament de Geologia, Universitat Autònoma de Barcelona, 08193 Bellaterra (Barcelona), Spain

Correspondence to: Florian Steinbach (florian.steinbach@uni-tuebingen.de)

Abstract. We performed numerical simulations on the micro-dynamics of ice with air inclusions as a second phase. ~~This provides first results of a numerical approach to model dynamic recrystallisation in polyphase crystalline aggregates.~~ Our aim was to investigate the rheological effects of air inclusions and explain the onset of dynamic recrystallisation in the permeable firn. The simulations employ a full field theory crystal plasticity code coupled to codes simulating dynamic recrystallisation processes and predict time-resolved microstructure evolution in terms of lattice orientations, strain distribution, grain sizes and grain boundary network. Results show heterogeneous deformation throughout the simulations and indicate the importance of strain localisation controlled by air inclusions. This strain localisation gives rise to locally increased energies that drive dynamic recrystallisation and induce heterogeneous microstructures that are coherent with natural firn microstructures from EPICA Dronning Maud Land ice coring site in Antarctica. We conclude that although overall strains and stresses in firn are low, strain localisation associated with locally increased strain energies can explain the occurrence of dynamic recrystallisation.

1 Introduction

The ice sheets on Greenland and Antarctica are composed of snow layers, originally containing a large proportion of air, which are transformed into solid ice due to compaction and sintering processes (Herron and Langway, 1980; Colbeck, 1983). At the firn-ice transition, the air is sealed off in bubbles as the pores are no longer connected and do not allow exchange with air from other layers or the atmosphere (Schwandner and Stauffer, 1984; Stauffer et al., 1985). For this reason, the ice sheets are considered as valuable archives of the paleo-atmosphere (Luethi et al., 2008; Fischer et al., 2008). However, ice sheets are not static, but flow under their own weight, which can potentially cause the paleo-climatic record to lose its integrity (Faria et al., 2010). For the interpretation of these records it is essential to not only understand the deformation dynamics of polycrystalline ice, but also the implications of a second phase in the form of air bubbles. For consistency, we use the expression *air bubbles* whenever referring to the natural material and *air inclusion* only for numerical models, where the individual units of air are neither interconnected, nor communicating.

Compared to other abundant minerals on the surface, ice on earth is always at ~~very~~ high homologous temperatures (T_h = $T_{actual}/T_{meltpoint}$), close to its pressure melting point and therefore creeping under gravitational forces (Petrenko and Whitworth, 1999; Faria et al. 2014a). The macroscopic behaviour of the ice aggregate results from the local response of individual ice crystals and the distribution of second phases within the polycrystalline aggregate.

Deformation in the ice crystal is mainly accommodated by dislocations, meaning intracrystalline lattice defects gliding and climbing through the crystal lattice, which is known as dislocation creep (Shoji and Higashi, 1978; Schulson and Duval, 2009; Faria et al. 2014b). Ice Ih is the ice polymorph that occurs on Earth. It has a hexagonal symmetry and dislocation glide is primarily on planes perpendicular to the c-axes (i.e. basal planes) or on pyramidal or prismatic planes. Dislocation glide in ice Ih is characterized by a strong visco-plastic anisotropy, with resistance to glide on basal planes at least 60 times smaller than on other planes (Duval et al., 1983). The strong preference for basal glide usually leads to an approximately single maximum crystallographic preferred orientation (CPO) with the c-axes mostly aligned with the direction of maximum finite shortening (Azuma and Higashi, 1985). Early experimental studies by Steinemann (1954) show, that such~~Such~~ a single-maximum CPO causes a mechanical anisotropy of a deformed aggregate of ice grains ~~(Budd and Jacka, 1989; Treverrow et al., 2012)~~. This is supported by experiments by Gao and Jacka (1987), the review by Budd and Jacka (1989) and more recent studies by Treverrow et al. (2012).

Visco-plastic deformation of ice is accompanied by recrystallisation (Duval, 1979; Jacka and Li, 1994; Faria et al. 2014b), as is common in minerals at high homologous temperatures. ~~According to Duval et al. (2000), r~~Recrystallisation processes have direct implications on creep behaviour as they affect fabric development and hence the flow of ice (~~Montagnat et al., 2011~~Duval and Castelnau, 1995; Castelnau et al., 1996; Duval et al., 2000). The nomenclature to describe recrystallisation and microstructure varies between glaciology, geology and material science. For consistency, in this manuscript we employ the terminology proposed by Faria et al. (2014b).

Under static conditions and non-deformation related, *normal grain growth* or static grain boundary migration driven by surface energy minimisation (Stephenson, 1967; Gow, 1969; Duval, 1985) leads to a microstructure with only slightly curved grain boundaries and 120° angles at grain triple junctions (foam texture). The resulting grain size distribution is log-normal according to (Humphreys and Hatherly, 2004, pp. 334-335). On the contrary, *strain-induced boundary migration* (*SIBM*) as described by Duval et al., (1983) or Humphreys and Hatherly (2004, pp. 251-253) minimizes stored strain energy by migrating boundaries towards less strained neighbouring grains. Intracrystalline annihilation of dislocations by lattice re-orientation into lower energy configurations, known as *recovery* (White, 1977; Urai et al., 1986; Borthwick et al., 2014), additionally lowers stored strain energies. Recovery accompanied by gradual formation of subgrain boundaries and ultimately new high angle grain boundaries (e.g. *polygonisation*, Alley et al., 1995) is termed *rotation recrystallisation* (Passchier and Trouw, 2005). These recrystallisation phenomena operate during deformation are summarized by the term *dynamic recrystallisation*.

Recrystallisation processes operate concurrently, but the proportion of contribution of each mechanism varies. The dynamic recrystallisation diagram by Faria et al. (2014b) describes the relative contributions as a function of strain rate and

temperature, as was done before for quartz (Hirth and Tullis, 1992). According to these models, rotation recrystallisation is more dominant with higher strain rates whereas strain-induced boundary migration dominates at higher temperatures.

In very shallow firn, at mass densities below 550 kg m^{-3}, compaction by displacement, re-arrangement and shape-change of snow particles is attributed to grain boundary sliding (Alley, 1987), neck growth between grains by isothermal sintering (Blackford, 2007) and temperature gradient metamorphism (Riche et al., 2013). Once the critical density is exceeded, the dominating mechanism becomes plastic deformation by intracrystalline creep (Anderson and Benson, 1963; Faria et al., 2014b). For the EPICA Dronning Maud Land (EDML) ice core, this critical density is reached at around 20 m depth (Kipfstuhl et al., 2009). However, more recent tomographic analyses on EDML samples by Freitag et al. (2008) provide evidence for an early onset of plastic deformation at shallow depths of 10 m. Simulations by Theile et al. (2011) suggest an even shallower onset of plastic deformation and the absence of grain boundary sliding.

One way to determine which deformation mechanisms operate~~d~~ is to study the microstructure of the deformed material (Passchier and Trouw, 2005; Kipfstuhl et al., 2009; Faria et al., 2014a, b). Apart from experiments, numerical simulations are increasingly used as a tool to establish the link between deformation mechanisms, boundary conditions and resulting microstructures (see review of Montagnat et al., 2014). Unfortunately, most studies on ice deformation only considered pure ice without air bubbles. Some exceptions are the experimental studies of Arena et al. (1997) and Azuma et al. (2012), or the numerical simulations of Roessiger et al. (2014) on grain growth of ice in the presence of air inclusions. Recent numerical modelling by Cyprych et al. (2016) indicates the importance of strain localisation in polyphase materials, but does not include a description of microstructure evolution during recrystallisation. Systematic numerical studies of the effect of a second phase, in this case air, on plastic deformation and concurrent microstructure evolution during dynamic recrystallisation are still lacking.

In this contribution we investigate the implications of air inclusions on deformation and recrystallisation to assess the importance of dynamic recrystallisation at shallow levels of ice sheets. For that purpose, we for the first time employ an explicit numerical approach combining both polyphase crystal plasticity and recrystallisation. Particular focus is given to two microdynamical aspects, which are (1) the strain distribution in the polyphase and polycrystalline ice-air aggregate and (2) its relation to (deformation induced) dynamic recrystallisation.

2 Methods

2.1 Multi-process modelling with Elle

We used the open-source numerical modelling platform Elle (Bons et al., 2008; Jessell et al., 2001; Piazolo et al., 2010), as this code is very suitable to model the interaction of multiple processes that act on a microstructure. So far, Elle has been applied to a range of microdynamic processes, such as strain localisation and porphyroclast rotation (Griera et al., 2011; 2013), deformation of polyphase materials (Jessell et al., 2009) or folding (Llorens et al., 2013a, b). Recent applications of ~~methods~~Elle codes utilized and updated for ~~also used in~~ this study are on dynamic recrystallisation in pure ice (Llorens et al.,

2016a, b), grain growth (Roessiger et al., 2011; 2014), and folding in ice sheets in relation to mechanical anisotropy, both on the small (Jansen et al., 2016) and large scale (Bons et al., 2016). To simulate visco-plastic deformation of the polyphase and polycrystalline aggregate with concurrent recrystallisation, the full field crystal visco-plasticity code VPFFT by Lebensohn (2001) was coupled to implementations of recrystallisation processes in Elle using the approach described in Llorens et al. (2016a, b). Here we only briefly explain the essentials of the modelling technique. The reader is referred to Jessell et al. (2001) and Bons et al. (2008) for the general principles of Elle. Details of the algorithms for grain boundary migration can be found in Becker et al. (2008) and Roessiger et al. (2011; 2014), and for coupled VPFFT and recrystallisation in Llorens et al. (2016a, b).

2.2 Discretisation of the microstructure

The two-dimensional microstructure of ice and air inclusions is discretised in a contiguous set of polygons with fully wrapping and periodic boundaries (Fig. 1a; Llorens et al., 2016a.b; Bons et al., 2008). In the setup used here, the polygons (termed *flynns*) are either ice crystals or air inclusions. Island grains such as a grain inside another grain are not allowed in Elle, for topological reasons. *Flynns* are delimited by straight segments that join boundary nodes (*bnodes*) in either double- or triple-junctions. Quadruple or higher-order junctions are also not allowed in Elle. Additionally, we superimpose a regular grid of unconnected nodes (*unodes*) on the set of *flynns*. *Unodes* store local state variables such as stress, normalized von Mises strain rate or dislocation density. Crystallographic orientations at *unodes* are defined by Euler triplet angles, following the Bunge convention. After each deformation increment, all state variables are mapped back to a regular, rectangular *unode* grid, as this is required by the VPFFT code. To track the finite deformation, a second set of *unodes*, on an initially regular square grid, represent material points or passive markers that are displaced each deformation step.

Topology checks are carried out at all times during a simulation to ensure compliance with topology restrictions and to maintain the set resolution. These include keeping *bnode* distances between a minimum and maximum separation by either deleting or inserting *bnodes* (Fig. 1b), and removing *flynns* that are smaller than a set minimum area or contain no *unodes* (Fig. 1c). To avoid the formation of a quadruple junction, a neighbour switch is performed between triple junctions closer than the minimum separation distance (Fig. 1c). When two sides of a *flynn* approach each other to below a set minimum distance, the *flynn* is split into two (Fig. 1e). This allows bulging grain boundaries to sweep across entire grains without causing overlapping *flynns*.

2.3 Visco-plastic deformation using full field approach

The full field crystal visco-plasticity code (VPFFT) by Lebensohn (2001) was coupled to the Elle numerical modelling platform following the approach by Griera et al. (2013) and Llorens et al. (2016a). The approach is based on calculating the mechanical field (i.e. stress, strain rate) from a kinematically admissible velocity field that minimizes the average local work-rate under the compatibility and equilibrium constraints (Lebensohn 2001; Lebensohn et al., 2009; Griera et al. 2013).

In this approach, intracrystalline deformation is assumed to be accommodate~~s~~d by dislocation glide on pre-defined slip systems, using a non-linear viscous, rate-dependent law. The strain rate $\dot{\varepsilon}_{ij}(\boldsymbol{x})$ at each position $\boldsymbol{x}$ (*unode*-position) in the grid is essentially the sum of the shear strain rates on all *N* slip systems (Eq. 1):

$$\dot{\varepsilon}_{ij}(\boldsymbol{x}) = \sum_{s=1}^{N} m_{ij}^{s}(\boldsymbol{x})\dot{\gamma}^{s}(\boldsymbol{x}) = \dot{\gamma}_0 \sum_{s=1}^{N} m_{ij}^{s}(\boldsymbol{x}) \left(\frac{m_{ij}^{s}(\boldsymbol{x})\sigma_{ij}'(\boldsymbol{x})}{\tau^{s}(\boldsymbol{x})} \right)^{3} \quad (1)$$

The constitutive equation relates the shear rate $\dot{\gamma}^{s}$ on each slip system (*s*), relative to a reference shear rate $\dot{\gamma}_0$, to the deviatoric stress σ_{ij}' and the orientation of the slip system that is defined by the symmetric Schmidt tensor m_{ij}^{s} (the dyadic product of a vector normal to the slip plane and slip direction). The effective viscosity or "ease of slip" of each slip system is defined by the slip-system dependent critical resolved shear stress τ^{s}. Here we use a stress exponent of three, assuming Glen's law (Glen, 1958).

Since the strain rate and stress fields are initially unknown, an iterative scheme is implemented with a spectral solver using a Fast Fourier Transformation. The VPFFT code provides the full velocity field, which is integrated to the displacement field for a small time step, assuming velocities remain constant. The displacement field is applied to the passive marker grid and to all *bnodes* to apply the deformation to the grains and air inclusions. Lattice orientations are updated and remapped onto the rectangular *unode* grid. Furthermore, geometrically necessary dislocation densities are calculated using the plastic strain gradient following Brinckmann et al. (2006) and assuming constant Burgers vectors for all slip systems.

2.4 Recrystallisation

2.4.1 Polyphase grain boundary migration

Polyphase grain boundary migration is modelled using a front-tracking approach, which is explained in detail by Becker et al. (2008) and Llorens et al. (2016a). Grain boundary migration is achieved by moving individual *bnodes*. In general, the movement $\Delta\boldsymbol{x}$ of a *bnode* is calculated from its mobility *M* and driving force *S* over a small numerical time step Δt:

$$\Delta x = SM(M_0, T(^{\circ}C))\Delta t \quad (2)$$

where the mobility *M* is a function of temperature *T* and intrinsic mobility M_0 (Nasello et al. 2005). The intrinsic mobility M_0 varies for different phase boundaries. The driving force *S* is calculated from the change in local free energy (*dE*) resulting from a change in position ($d\boldsymbol{x}$) of the *bnode* under consideration. *dE* is a function of the change in boundary length and, hence, total local grain-boundary surface energy (Becker et al. 2008) and the change in stored strain energy (Llorens et al. 2016). A *bnode* is moved (using Eq. 2) in the direction of maximum free-energy reduction, which is determined from four small orthogonal trial displacements of that *bnode*. For the movement of ice-air boundaries, the stored strain energy was not taken into account.

In a polyphase aggregate, the conservation of mass requirement influences boundary migration. In theory, any local movement of a boundary needs to conserve the cross sectional area of its host grain. This restriction would inhibit most ice-air interface movements, prohibiting any geometrical changes of air inclusions. Therefore, an additional energy term (E_{area}) is introduced to counter-act that the surface energy (E_{surf}) would drive an ice-air boundary inwards and let air inclusions shrink (Roessiger et al., 2014). For ice-air boundaries, the total local energy (E_{total}) at a given trial position j only depends on the surface energy change and the relative area change resulting from a theoretical movement of the boundary node to this position:~~stored strain energy is not taking into account and the total local energy (E_{total}) at a given trial position j then depends on the relative area change resulting from a theoretical movement of the boundary node to this position:~~

$$E_{total}(j) = E_{surf}(j) + E_{area}(j) \quad (3)$$

$$E_{area}(j) = c\left(\frac{A(j) - A_0}{A_0}\right)^2 \quad (4)$$

where A_j is the area of the air inclusion when the *bnode* is at trial position j and A_0 is the initial inclusion area. Decreasing c essentially increases the accepted violation of the conservation of mass requirement, allowing a stronger change in cross sectional area. For the polyphase aggregate of ice and air, the pre-factor c can be regarded as a compressibility factor: Theoretically, surface energy drives the bubble surface inward, compressing the enclosed air and increasing the air pressure in the bubble. This pressure would counter-act the surface movement until an equilibrium between surface tension and inner bubble pressure is reached, leading to a stable bubble cross sectional area. The factor c controls how quickly this equilibrium is reached.

To fulfil the conservation of mass requirement, any movement of the interface that is not mass conserving should be inhibited. However, this would cause a locking of the ice-air interface and inhibit any changes in inclusion shape. Therefore, we allow movements that conserve the overall fraction of air, but allow for sufficient shape changes of the bubbles. Preparatory tests yielded c = 0.1 as a compromise achieving this equilibrium. This assumption will inhibit almost all porosity changes during the simulation, causing our approach to assume an incompressible air inclusion, which does not allow us to quantitatively compare the modelled inclusion shapes or sizes with natural samples that experienced compaction. This limitation is further discussed in section 4.5.

We chose to use most input parameters from published literature to allow comparability of the results to previous modelling. Following the experimental results of Nasello et al. (2005), the intrinsic mobility $M_{ice\text{-}ice}$ of ice-ice boundaries was set to 0.023 $m^4\ J^{-1}\ s^{-1}$, which Nasello et al. (2005) determined for slow movement and is consistent with previous modelling by Llorens et al. (2016a,b). A slower movement is more suitable for our simulations as a higher mobility would cause numerical errors when using the same time step. Furthermore, it mitigates the effect of large numerical grain sizes (section 4.5). The grain boundary mobility was determined as a function of temperature and intrinsic mobility according to Nasello et al. (2005). To be consistent with previous modelling, the surface energy $\gamma_{ice\text{-}ice}$ of ice-ice boundaries was set to 0.065 J m^{-2}, as

commonly used in the literature (Ketcham and Hobbs, 1969; Nasello et al., 2005; Roessiger et al., 2014; Llorens et al. 2016a,b). Based on Roessiger et al. (2014), the mobility ratio of ice-ice and ice-air boundaries $M_{ice\text{-}ice}/M_{ice\text{-}air}$ was set to 10, which in their study provided results in compliance with the experimentally derived grain growth rates of Arena et al. (1997). The surface energy $\gamma_{ice\text{-}air}$ for ice-air boundaries was set to 0.52 J m^{-2}, which as a function of ice-ice surface energies ($\gamma_{ice\text{-}ice}$) results in a dihedral angles of 173° and almost circular air inclusions (Roessiger et al., 2014).

~~Grain boundary mobility is a function of temperature and intrinsic boundary mobility. Following the results of Nasello et al. (2005), the intrinsic mobility $M_{ice\text{-}ice}$ of ice-ice boundaries was set to 0.023 m^4 J^{-1} s^{-1} and their surface energy $\gamma_{ice\text{-}ice}$ to 0.065 J m^{-2} (Ketcham and Hobbs, 1969). Based on Roessiger et al. (2014), the mobility ratio of ice-ice and ice-air boundaries $M_{ice\text{-}ice}/M_{ice\text{-}air}$ was set to 10 and the surface energy $\gamma_{ice\text{-}air}$ of ice-air boundaries to 0.52 J m^{-2}. This causes a dihedral angle of 173° at ice-air triple junctions. For all simulations, c was set to 0.1.~~

In a two-phase model, such as ice with air inclusions, three boundary types are possible: Ice-ice, air-ice and air-air boundaries. Air-air boundaries can occur in the model, for example when two air inclusions merge into one. These boundaries are purely numerical and have no physical meaning. They are therefore excluded them from any modelling processes or post-processing analyses.

During the simulation, all *bnodes* are selected in a random order and moved according to Eq. (2) one at a time. After each movement, topological checks are performed in keeping with the topological restrictions of Elle and to avoid impossible topologies such as *bnodes* sweeping across other grain boundary segments. Once a *unode* is swept by a moving boundary and thus changes its host grain, its dislocation density is set to zero and its lattice orientation to the value of the nearest neighbour *unode* in the new host grain.

2.4.2 Rotation recrystallisation

The process of rotation recrystallisation is modelled in two separate steps during the multi-process simulation: (1) Recovery bey rearranging the intracrystalline lattice orientations into lower energy configurations such as subgrain boundaries, which is the predecessor for (2) the creation of new grains defined by high angle boundaries, which here implies inserting new boundary nodes and splitting an existing *flynn*.

In analogy to the grain boundary migration code, an energy minimisation system is used. Each *unode* is regarded as a small crystallite characterized by a lattice misorientation with respect to its first-order neighbours. Misorientation is the difference in lattice orientation between two *unodes*, which increases the total free energy of the local system. Small trial rotations are used to determine which lattice rotation would result in the maximum decrease in local free energy. The lattice in the *unode* is then rotated according to this decrease and a "mobility" term, as described in detail in Borthwick et al. (2014) and Llorens et al. (2016a).

Both the visco-plastic deformation and the above recovery process lead to polygonisation, i.e. the formation of new high-angle grain boundaries defined by a lattice misorientation between neighbouring *unodes* that exceeds a critical angle α_{hagb}. Such new grain boundaries are initially not defined by *bnodes*, and are thus numerically excluded from grain-boundary

migration (Section 2.4.1). Polygonisation requires the creation of new high angle grain boundaries by splitting an existing *flynn* and inserting new boundary nodes. When intragranular misorientations that exceed α_{hagb} are detected, grain splitting is activated. This is achieved by finding clusters of *unodes* with common lattice orientations, separated by high-angle boundaries. The positions of the new boundary nodes are found using a Voronoi decomposition of the *unode* clusters, storing the Voronoi points surrounding the cluster as new *bnodes*. The critical angle α_{hagb} has been suggested to be 3 to 5° for ice Ih, based on experiments that combine grain boundary properties and high-angular resolution measurements (Weikusat et al., 2011a, b). Here we use α_{hagb} = 5° as a conservative estimate. Lower angles would lead to smaller grain sizes, which potentially cause more topological problems.

2.5 Process coupling

Multi-process modelling of polyphase deformation and recrystallisation is achieved by operator splitting. In Elle, the specific physical processes that contribute to microstructure evolution are programmed as standalone modules. These are coupled by a control program, successively running them in isolation, each for a short numerical time step (Fig. 2a). The numerical setup takes into account the visco-plastic deformation (Section 2.3) and dynamic recrystallisation (DRX, Section 2.4) which here covers grain boundary migration, recovery and polygonisation.

The recrystallisation modules are computationally less expensive but require short numerical time steps. To reduce numerical errors, the time step for recrystallisation processes is set 20 times smaller than for deformation (VPFFT). In accordance with the smaller time step, one simulation step comprises one VPFFT step and five subloops that run the recrystallisation codes four times per subloop. This adds up to 20 times more recrystallisation steps than VPFFT steps, but an equal time step for all physical processes. Systematic studies showed that the order of the processes as illustrated in Fig. 2a has no significant influence o~~f~~n the results using the properties described above.

2.6 Setup of simulations

Three starting microstructures were used to investigate the effect of visco-plastic deformation and DRX at different area fractions of air inclusions of 0 %, 5 % and 20 % air phase, termed F00, F05 and F20, respectively (Fig. 2b). In general, we refrain from relating our air fractions to specific depth or porosity ranges in firn or ice as our approach is limited and assumes an incompressible air phase. We chose to use these settings to represent only approximate ice-air aggregates as found in firn (F20) and well below the firn-ice transition (F05) and used simulation F00 for reference. With this, we do not limit our study to firn, but to ice-air aggregate in general. All initial microstructures were created from the same 10x20 cm² foam texture with 3267 grains. With this, the intial mean grain sizes of our modelling were larger than typical firn mean grain sizes as presented in e.g. Kipfstuhl et al. (2009), but consistent with previous simulations by Llorens et al. (2016a,b). Lattice orientations were mapped onto a regular grid of 256x256 *unodes* with a random initial lattice orientation assigned to each grain. Air inclusions were introduced by setting air properties to the desired area percentage of grains, followed by running solely surface-energy based (static) polyphase grain boundary migration until air inclusion sizes equilibrated in area

and shape~~, using an area energy factor c = 0.1.~~ For consistency, for this static grain boundary migration, the same area energy factor c = 0.1 (Eq. (4)) as for the actual dynamic recrystallisation and deformation simulations was used. Section 4.5 discusses the use of this factor in more detail.

The three starting microstructures were deformed in pure shear with a constant incremental strain of 1% vertical shortening over 75 simulation steps. Each simulation step comprised 20 recrystallisation steps per VPFFT step and equalled 10^8s = 3.16 yrs, resulting in a vertical strain rate of 10^{-10} s^{-1} and deformation up to 53% vertical shortening. We remark that the modelled strain rate is about an order of magnitude faster than assumed for firn at the EDML site (Faria et al., 2014b) and that modelling a slower strain rate is possible, yet currently too numerically expensive. From a technical point of few, fast strain rates have the advantage that the time steps for recrystallisation routines can be small. To achieve slower strain rates, the number of recrystallisation steps per deformation step would need to be increased at a significant expense of computation time.

Dislocation glide was assumed for ice Ih crystallography with slip on basal, pyramidal and prismatic planes, using a ratio of basal to non-basal critical resolved shear stresses of $\tau_{basal}/\tau_{non\text{-}basal}$ = 20. Air was modelled as an incompressible crystalline material with the same crystallography and slip systems as for ice, but with $\tau_{s\text{-}air}$ set 5000 times smaller than τ_{basal} of ice. Hence, as for ice Ih, deformation in the air phase was also resolved on basal, pyramidal and prismatic planes which were characterized by equally small critical resolved shear stresses. This leaves the air phase slightly anisotropic as the deformation is restricted to these defined slip planes. However, this approximation does not significantly affect the results (section 4.5 and supplementary figure S2). With this ~~assumption~~treatment of the air phase, the stress in points belonging to pores can be considered to nearly vanish compared to stresses reached in the solid grains, which is coherent with results from modelling of void growth using a dilatational visco-plastic FFT-based formulation (Lebensohn et al, 2013). The simplification of assuming incompressibility allowed us to exclude the effect of compaction during microstructure evolution and is further discussed in section 4.5.

Temperature throughout the simulations was assumed constant at -30 °C. A detailed summary of all input properties can be found in Table 1. Where not indicated differently, we employed input parameters as used by Llorens et al. (2016a, Table 1).

For comparison of grain size statistics, we additionally performed three normal grain growth (NGG) simulations using solely surface energy driven grain boundary migration and no deformation. The NGG simulations used the three microstructures for F00, F05 and F20 as presented in Fig. 2b and the numerical time step was kept the same as in the deformation simulations.

2.7 Post processing ~~and microstructure imaging~~

2.7.1 Strain rate and strain localisation quantification

In order to visualize and explain the simulations, some post-processing steps were necessary. Strain rate tensor fields predicted by FFT were transformed in *von Mises equivalent strain rates* normalizing the von Mises strain rate for each *unode*

to the bulk value of the whole model. The von Mises strain rate $\dot{\varepsilon}_{vM}$ provides a scalar measure of strain rate intensity and was calculated as a function of the symmetric strain rate tensor:

$$\dot{\varepsilon}_{vM} = \sqrt{\frac{2}{3}\dot{\varepsilon}_{ij}\dot{\varepsilon}_{ij}} \quad (5)$$

In addition, we quantified strain localisation at each step during the simulation. Analogous to Sornette et al. (1993) and Davy et al. (1995), the degree of localisation *F* was calculated with:

$$F = 1 - \frac{1}{N_u}\frac{(\sum \dot{\varepsilon}_{vM})^2}{\sum \dot{\varepsilon}_{vM}^2} \quad (6)$$

where N_u is the total number of *unodes* within ice grains and $\dot{\varepsilon}_{vM}$ the von Mises equivalent strain rate of each *unode*. The localisation factor *F* ranges from 0 to 1, such that 0 represents completely homogeneous deformation and 1-1/ N_u maximum localisation, where all strain is accommodated by a single *unode*. Note that Sornette et al. (1993) and Davy et al. (1995) used a slightly different localisation factor *f*=1-*F*, where 1 represents homogeneous deformation.

2.7.2 Driving forces and crystallographic orientations

For each step of grain boundary migration, the driving forces for migration were stored in *bnode* attributes differentiating between surface and stored strain energy driving forces. Details about the driving force calculation can be found in Llorens et al. (2016a, equations 10-12). By normalizing the local stored strain energy to *bnode* mean surface energy, we obtained a quantitative measure of how much grain boundary migration is induced by strain energy. For each simulation step, the *bnodes* only stored the driving forces for the last grain boundary migration step. This allowed to capture the correct driving forces at the end of the simulation step after a time increment during which strain energy was induced by deformation and reduced by recrystallisation processes. Hence, we determined a minimum estimate for strain energies, which may have been higher in an intermediate stage of the simulation step.

Crystallographic preferred orientations were stored and updated during the simulations. Pole figures and Eigenvalues were extracted using the texture analysis software MTEX (Bachmann et al., 2010; Mainprice et al., 2011) based on the orientation distribution function. The projection plane was chosen to be parallel to the x-y plane of the numerical model and c-axis orientation was expressed using the angles of azimuth and dip in this plane.

~~**2.7.3 Microstructure mapping of natural samples**~~

~~To qualitatively compare the simulation results to natural firn microstructures, we utilized an image from a firn sample taken from the EPIA-Dronning Maud Land ice core (EDML) site, Antarctica. The sample was cut from a core from 80 m depth. Using density and annual layer thickness data of Kipfstuhl et al. (2009) for the EDML core, the density is about 800 kg/m^3 at~~

~~80 m depth and the total vertical shortening up to 50% (Faria et al., 2014b estimated this value based on the supplementary material from Ruth et al., 2007). A plane was cut from the sample and prepared for microstructure mapping (Kipfstuhl et al., 2009). The microstructure mapping technique allows detailed imaging of ice, air bubbles, (sub-) grain boundaries and other microstructural features typically found in polar ice. It is based on keeping a polished sample surface in a cold, yet dry environment, causing preferred ice sublimation at (sub-) grain boundaries. After sublimation, the prepared sample surface is scanned using a Large area scan macroscope (Krischke et al., 2015) highlighting topographical changes on the surface in a grey scale image.~~

3 Results

Table 2 and Fig. 3 provide an overview of the results obtained from simulating pure shear deformation with ongoing recrystallisation for three different amounts of air inclusions. Selected movies illustrating the full microstructure evolution can be found as supplementary material in the AV Portal of TIB Hannover (av.tib.eu). The resulting microstructures are characterized by heterogeneous grain size distributions and a slight increase in average grain sizes compared to the initial one. Most grains have smoothly curved boundaries and are usually equidimensional to slightly elongate in the *x*-direction. Coalescence of air inclusions (Roessiger et al., 2014) led to a number of large inclusions in simulation F20. The largest air inclusions show a marked elongation, mostly oblique to the shortening direction. Small inclusions remained circular.

The strain and strain rate distribution is difficult to discern from the final air inclusion and grain shapes only, as these are constantly reworked by DRX (Llorens et al., 2016b). Instantaneous strain rate maps and finite strain passive marker grids provide better insight in deformation heterogeneity (Fig. 3), which is also visible in movies that show the whole deformation history (AV Portal of TIB Hannover, av.tib.eu). Strain localisation is observed in all simulations independent of the presence of air inclusions. While instantaneous strain rate maps (Fig. 3b) can only show localisation at the current time step, passive marker grids reflect the accumulated strain throughout the microstructure evolution (Fig. 3a-b). Figure 3b shows that zones with high strain rates, are oriented at ≤45° to the shortening direction. Zones with a high finite strain, or shear bands, are visible in the finite-strain pattern. These zones of accumulated shear strain initially formed at ca. 45° and subsequently rotated away from the shortening direction, especially in air-free ice (F00). High strain (-rate) zones form bridges between air inclusions when these are present. Regions between the high strain zones are characterized by both low strain rates and low accumulated finite strains.

Using the localisation factor *F*, it is possible to quantify the degree of strain localisation in our simulations. Figure 4 shows the evolution of this factor with strain for all simulations. In accordance with strain rate maps and passive marker grids, non-zero ($F \geq 0.3$) values are observed throughout the simulations, indicating strain localisation in all cases. *F* increases up to about 40% vertical shortening, after which the rate of increase is lower. Localisation increases with the amount of air inclusions, with $F \approx 0.5\text{-}07$ in simulation F20 about double that for pure ice ($F \approx 0.3\text{-}0.35$).

To investigate the competition between surface and stored strain energies in grain boundary migration, the strain energy driving forces for simulation F20 were normalized to mean surface energies and plotted for each *bnode* (Fig. 5a). The colour scale is adjusted to plot *bnodes* without a contribution of strain-induced energies in the background colour (blue). Boundaries with a significant contribution of stored strain energies are indicated by green to red colours. A comparison with Fig. 3 shows that grain boundary migration that is driven mostly by strain energy (bright colours) are predominantly located in high strain (-rate) zones. Examples are indicated by large arrows in Fig. 5a and between three elongated and large air inclusions in the lower middle region of the final microstructure of F20. Conversely, the contributions of surface and strain energy to grain-boundary migration are about equal in less-strained areas.

Qualitatively, microstructure images show a heterogeneous grain size distribution (Fig. 3). To further visualize the spatial distribution of grain sizes, the microstructure in Fig. 5b shows ice grains coloured according to their area. Analogous to the driving force distribution for grain-boundary migration, we observe the smallest grains between air inclusions coinciding with zones of marked strain localisation.

Figure 6 depicts ice grain size statistics for the final microstructures. To visualise the influence of dynamic recrystallisation, grain size histograms are compared with normal grain growth (NGG) simulation results. All simulations show an increase of average grain areas with respect to the initial mean grain sizes (Fig. 6, Table 1). However, dynamic recrystallisation simulations resulted in a grain size distribution skewed towards smaller grain sizes than for NGG simulations. Furthermore, the distribution of grain sizes is broadened when dynamic recrystallisation was active. With increasing amount of air in simulations F05 and F20, the average grain-size increase compared to the initial state is lower for both dynamic recrystallisation and NGG results.

Crystallographic preferred orientations in simulations are visualised using pole figures and maps of c-axis azimuths (Fig. 7). The evolution of orientations is also illustrated in movies to be found in the AV Portal of TIB Hannover (av.tib.eu). After 53% of vertical shortening, the initially random fabric is re-arranged with c-axes preferentially oriented parallel to the vertical shortening direction (Fig. 7a). This maximum becomes less pronounced with increasing amount of air as reflected in pole figures and quantified by a decrease in first eigenvalues of the orientation distribution from 0.80 (F00) to 0.69 (F20). This trend is also visible in c-axis orientation maps (Fig. 7b), which shows a more heterogeneous distribution of well-aligned and random fabrics with increasing air content. Most grains in simulation F00 have c-axes azimuths parallel to the y-axis. Grains within high strain bands by a slight tilt of the c-axes to the left or right, depending on the orientation of the shear bands. In contrast, simulation F05 and, even more, F20 show areas of small grains with c-axes strongly aligned perpendicular to high strain bands (white arrows in Fig. 7b). This means that the basal planes are aligned parallel to these bands. In low strain areas, such as the middle part of the F20 model, a much more random c-axis distribution is observed (white circle in Fig. 7b) compared to simulation F00.

~~For comparison with natural ice and firn core examples, a microstructure image from 80 m depth from the EDML site was provided. Apart from the scale difference, the F20 and EDML microstructure show some distinct similarities (Fig. 8), in particular in the heterogeneity in grain shape and size distribution. Detail area A in Fig. 8 contains larger grains, with more~~

~~120° angles at triple junctions and a lower density of subgrain boundaries than area B between bubbles. Similar areas can be found in simulation F20. While area C has large grains with straight grain boundaries and 120° angles at triple junctions (comparable to A), area D is characterised by small grains between the bubbles that are occasionally elongated and show other triple junction angles (comparable to B). As an estimate for subgrain boundary density, average misorientation between *unodes* was plotted underneath the grain boundary network. In detail image D, we observe a higher density of subgrain boundaries as illustrated by higher average misorientations than in area C.~~

4 Discussion

4.1 Strain localisation

Our simulations indicate a distinct strain localisation in both pure ice and ice with bubbles. Strain localisation is not a transient effect, but actually increases, at least up to about 40% of strain (Fig. 4). Strain localisation in pure ice (F00) is related to the plastic anisotropy of the ice crystal. Grains, or clusters of grains, with initially suitable orientations for slip accommodate strain more efficiently and thus initiate the first regions of strain-rate localisation. With progressive strain these localisation zones may strengthen as the basal planes align themselves with the local shear plane, or they are deactivated when either the internal lattice orientations or the orientation of the localisation zones become less suitable for further localisation. Once deactivated, the localised zones only rotate and move passively with the bulk deformation, and may remain visible as shear bands in the finite strain grid. Our observation of strain localisation in a polyphase aggregate is consistent with numerical models by Cyprych et al. (2016), who predict strain localisation as an important mechanism in polyphase materials, such as ice with soft or hard inclusions.

In the presence of air inclusions, localisation zones are forming at bridges between the inclusions where stresses are highest. Even in the absence of plastic anisotropy this leads to the formation of localisation zones, especially in power-law materials (Jessell et al., 2009). With increasing air fraction, the arrangement and geometry of air inclusions become the main controllers of strain localisation in the ice-air aggregates and crystallographic orientations exert only a secondary control. The additional localisation mechanism causes stronger localisation in ice with air than without air.

The localisation zones enclose lozenge-shaped areas of low strain rate, which we term *microlithons*, in keeping with terminology used in geology (e.g. Passchier and Trouw, 2005 p. 78). In pure ice, the CPO within the microlithons is strong and trends towards a single maximum fabric. With air inclusions causing intensified strain localisation, the CPO is expected to be more heterogeneous with differences between high- and low-strain rate zones. Within localisation zones, the basal planes rotate towards the local shear plane, causing a divergence of the c-axes azimuths away from the vertical compression direction. This is in contrast to the microlithons, in which CPO development is slower because of the relatively low strain rate. The weaker bulk single-maximum fabric with increasing amount of air is thus an effect of air inclusions causing distinctly localised zones that accommodate most of the deformation, and less deformed microlithons that preserve the initial fabric. Our results are an illustrative example of the role of second phases on CPO development. If the weak phase is the

secondary phase and the strong phase is load bearing, as in our simulations, strain localisation controlled by the distribution of second-phase inclusions. This produces a locally weaker CPO in the microlithons, but also in the bulk material.

Grain boundary sliding is assumed to be an explanation for a weaker CPO in polyphase materials (e.g. Fliervoet et al., 1997). However, a weaker CPO with increasing content of the second phase is found in our simulations, in the complete absence of grain-boundary sliding. Therefore, a weaker CPO alone should not be regarded as unambiguous evidence for grain-boundary sliding. This supports studies indicating a very shallow onset of plastic deformation in the ice sheets (Freitag et al., 2008) and absence of grain boundary sliding (Theile et al., 2011).

4.2 Natural firn microstructures and numerical simulations

For comparison with natural ice and firn core samples, a microstructure image from 80 m depth from the EDML site is used (Fig. 8). For this image, a 2D sample was vertically cut from the firn core, and processed for microstructure mapping as described in Kipfstuhl et al. (2006; 2009) using a large area scan macroscope (Krischke et al., 2015). Here, we refrain from any detailed or quantitative comparison of our numerical simulations with respect to grain sizes, bubble size, shape or distribution. Such comparisons are hindered by model assumptions such as assuming an incompressible air phase or area conserving pure shear deformation (section 4.5). We observed air inclusions coalescing during our simulations. This is expected from static polyphase grain-growth simulations by Roessiger et al. (2014), but may be suppressed in firn as simultaneous shrinkage of bubbles may hinder them from touching and merging.

The F20 and EDML microstructure show qualitative similarities (Fig. 8), in particular in the heterogeneity in grain shape and relative grain size distribution. As an estimate for numerical subgrain boundary density, average misorientation between unodes was plotted together with the grain boundary network. In case of natural firn, detail area A (Fig. 8) contains larger grains, with more 120° angles at triple junctions and a lower density of subgrain boundaries than area B, which is characterized by a higher density of bubbles. Visually, similar areas can be found in simulation F20. Area C has large grains with straight grain boundaries and 120° angles at triple junctions and lower misorientations (qualitatively comparable to A), and area D is characterised by small grains relative to C. Triple junction angles in D differ from 120° and D has higher internal misorientations (qualitatively comparable to B). The grain sizes can only be compared relatively, as mean grain size in simulation and sample differ. Besides, this natural sample is a 2D slice through a 3D body, but the simulations are purely 2D. For more rigorous comparisons, corrections for stereologic issues are required.

With respect to the limitations of the modelling approach (section 4.5), we cannot quantitatively compare the simulations to natural firn. However, as detail D (Fig. 8) is marked by higher finite strains related to strain localisation and is indicates more influence of dynamic recrystallisation as presented by Kipfstuhl et al. (2009), similar processes may have controlled the natural microstructure in detail image B (Fig. 8). On the contrary, the natural ice in detail A probably experienced lower finite strains, as suggested from a comparison with the numerically modelled detail image C (Fig. 8). As strain localisation and the resulting heterogeneity in finite deformation pattern can be masked by grain boundary migration in natural ice

(Llorens et al. 2016b), our numerical simulations can help to visualise the actual heterogeneity within the structure, leading to an improved understanding of how dynamic recrystallisation is distributed within the ice-air aggregate.

4.2~~2~~3 Implications of strain localisation for the occurrence of dynamic recrystallisation

According to published deformation mechanism maps (Shoji and Higashi, 1978; Goldsby, 2006), dislocation creep is to be expected for the average grain size, strain rate and temperature of our simulations. Also, the effective density of the simulation F20 (approximately 750 kg m^{-3}) is above the critical density of 550 kg m^{-3} where plastic deformation via dislocation creep is classically supposed to dominate (Maeno and Ebinuma, 1983). Therefore, we assume that our model assumption of deformation accommodated by dislocation creep only is sufficient to draw conclusions on mechanisms acting at comparable densities and depth in nature.

With the assumption of dislocation glide as the only strain accommodating mechanism, the dislocation density is expected to increase unless recovery reduces densities by re-arrangement of misorientations in lower energy configurations. A localisation in strain results in higher strain gradients at the localisation zone margins and hence locally higher strain energies. It is therefore associated with locally enhanced strain-induced boundary migration, as can be seen in Fig. 5a. This is in accordance with Weikusat et al. (2009) stating that strain-induced boundary migration occurs localized and the driving forces have to be considered locally. Duval (1985) argued that the strain energy in firn should be small in comparison with surface energies and Duval and Castelnau (1995) conclude that strain induced boundary migration is most dominant for ~~a~~ temperature~~s~~ of -10 °C or higher~~. is essential for strain induced boundary migration.~~ This led to the assumption by De la Chapelle et al. (1998) that dynamic recrystallisation is essentially restricted to the basal part of ice sheets and therefore an improbable process in firn.

Faria et al. (2014b, p. 45) theoretically discuss the relation of strain localisation to localized dynamic recrystallisation in firn. They state that although the overall stresses and strains in firn are low, it is "characterised by large strain variability" and locally highly increased stresses and strains depending on the geometry of the air bubble network. They further conclude that stored strain energy could be very high in *particular* regions of the ice skeleton causing dynamic recrystallisation to start in shallow levels. Our simulations are coherent with this statement and confirm the theoretical predictions by Faria et al. (2014b).

Since improving microstructural imaging methods by Kipfstuhl et al. (2006) gave further insight in firn microstructures, studies by Weikusat et al. (2009) and Kipfstuhl et al. (2009) gave microstructural evidence for dynamic recrystallisation in shallow parts of the ice column and firn. In contrast to assumptions by for instance De la Chapelle et al. (1998), it therefore seems probable that dynamic recrystallisation already takes place at very shallow levels in the ice sheet, at least in localised zones. Our simulations at -30°C as well as observations of natural firn microstructures at EDML ice coring site (Kipfstuhl et al. 2009~~, Fig. 8~~) with approximately -45°C annual mean temperature (Oerter et al. 2009), indicate that even at low temperatures deformation is providing enough energy to allow for strain induced grain boundary migration.~~the initiation of this process is not only temperature dependent. It~~ The relative dominance of this process is also a function of strain rate,

since locally high strain rates and stress concentrations at bridges between the air inclusions induce high driving forces. This is in accordance with the recrystallisation diagram by Faria et al. (2014b), in which the occurrence of recrystallisation mechanisms is essentially a function of temperature and strain rate (i.e. work rate, which is the product of stress and strain rate), rather than depth.

~~Our numerically modelled microstructures resemble patterns observed in natural firn microstructures from EDML site (Fig. 8), supporting the microstructural evidence for the occurrence of dynamic recrystallisation in firn from the EDML ice core site (Kipfstuhl et al., 2009). However, the scale differs with the mean grain size in the models about one order of magnitude larger than in the EDML sample. It should be noted that the experimental strain rate (10^{-10} s^{-1}) is also about ten times larger than the $7.4 \cdot 10^{-12}$ s^{-1} strain rate estimated for the sample (Faria et al., 2014b).~~

~~It should be noted that the strain rate in our simulations (10^{-10} s^{-1}) is an order of magnitude faster than assumed for the 80 m deep sample from the EDML core (Faria et al., 2014b). Modelling a slower strain rate is possible, but currently too time consuming. From a technical point of view, fast strain rates lead to numerical error reduction as the time steps for recrystallisation codes can be low. To achieve slower strain rates at the same time step, the number of recrystallisation steps per deformation step needs to be increased at a significant expense of computation time.~~

According to the dynamic recrystallisation diagram by Faria et al. (2014b), a lower strain rate would decrease the contribution of rotation recrystallisation and increase that of strain-induced grain boundary migration to the final microstructure. This would reduce the difference in grain size between high- and low-strain zones. A difference variation in grain size is, however, still observable in the EDML sample, indicating that grain-boundary migration was not able to obliterate the effects of rotation recrystallisation in these suspected high-strain zones, even at the lower natural strain rate.

Because of dynamic recrystallisation, grain shapes are mostly equidimensional, even in the highest-strain bands. Recrystallisation thus masks the localisation in the microstructure (Llorens et al., 2016b), making it difficult to discern strain localisation in natural samples. Subtle indications of localisation may, however, be zones with a deviating lattice orientation (Fig. 7) (Jansen et al., 2016) or zones with a smaller grain size (Fig. 5b). In single phase ice, where localisation zones shift through the material, only the youngest localisation zones may be visible, as the microstructure is reset in extinct localisation bands (compare simulation F00 in Fig. 3 and 7) (Jansen et al., 2016). Since bubbles fix the locations of shear localisation, their presence may be more obvious in natural samples, such as the one from the EDML (Fig. 8). In general, bubbles may only be useful to discern localisation zones (as in F20), if the bubbles are large and strain rates are high enough, which will cause elongated bubble shapes.~~Only if bubbles are large and strain rates high enough the elongate shape of the largest bubbles can be used to discern localisation zones (simulation F20).~~

4.~~3~~ 4 Grain size analyses

We refrain from a detailed comparison of our grain-size data and those observed in nature as a discussion of the stereologic issues related to our 2D model and sections through 3D natural samples would be beyond the scope of this paper. Furthermore, the limitations of the current modelling approach such as the large initial grain size, requirement of fast strain

rates and incompressibility of air inclusions does not allow for such a detailed quantitative study. Still, the grain size statistics of the simulation results provide a comparison between the distribution for the non-deformation related normal grain growth (NGG) and deformation induced dynamic recrystallisation with varying amounts of air.

~~Grain size statistics of the simulation results provide a comparison between the distribution for the non-deformation related normal grain growth (NGG) and deformation induced dynamic recrystallisation with varying amounts of air.~~ An increase in grain size is observed in all ~~cases~~simulations, but less for dynamic recrystallisation and also less with an increasing amount of air inclusions. The observation of a lower final grain sizes for higher amounts of air is related to the growth regimes presented by Roessiger et al. (2014) based on numerical simulations on NGG in ice-air aggregates: (1) The first regime is characterised by ice grain sizes ~~lower~~ less than bubble spacing, where most grains can grow unhindered by bubbles as in single phase polycrystalline ice. The growth rate is constant. (2) The second regime is a transitional regime, where bubble spacing is close to the grain diameter and the growth rate decreases. (3) In the third regime, all grains are in contact with bubbles. A slow, but steady growth rate is reached again, controlled by the coalescence rate of bubbles that increases their spacing. In our case, NGG in the simulations with air inclusions is slowed down, indicating regime (2) growth with a small, but significant fraction of the grains in contact with inclusions, and thus hindered in their growth (Fig. 6).

In comparison with NGG simulations, our VPFFT simulations with dynamic recrystallisation show smaller final grain sizes and broader distributions. The broadening reflects the microstructural heterogeneity induced by dynamic recrystallisation (in particular grain splitting during rotation recrystallisation) and strain localisation. Locally, grains size has remained small due to rotation recrystallisation, whereas in other, low strain-rate regions, grain sizes have increased. Here surface energy constituted a significant, if not dominant, proportion of the driving force for grain boundary migration. These results are consistent with the observed broadening of the grain size distribution with depth in firn from the EDML site (Kipfstuhl et al., 2009), accompanied by an increasing number of deformation-related substructures such as subgrain boundaries and irregular boundary shapes. Our modelling confirms the interpretation by Kipfstuhl et al. (2009) that this trend is related to the onset of dynamic recrystallisation. ~~We refrain from a detailed comparison of our grain size data and those observed in nature as a discussion of the stereologic issues related to our 2D model and sections through 3D natural samples would be beyond the scope of this paper.~~

4.5 Limitations of the modelling approach

In our polyphase simulations, air inclusions are modelled as an incompressible material. By imposing pure shear, we assume a deformation mode that conserves the total area and in turn the mass of both phases. However, in natural firn, most of the vertical thinning is achieved compaction. Compaction is a function of the surface energy driving movement of the ice-air interface and the counter-acting inner bubble pressure that depends on overburden pressure and bubble size and shape. Our model assumes equilibrium between those pressures leading to a stable fraction of air. This is controlled by the area energy that is incorporated in the pre-factor c. The lower this factor, the more influence of surface energy is allowed and the more the conservation of mass requirement is violated as more inward movement of the ice-air interface is allowed. The pre-factor

constant c (Eq. 4) was adjusted to allow slight changes in cross sectional area that keep the overall amount of air in the model constant, but compensate shape changes due to deformation to maintain an approximately circular bubble shape and allowing bubbles to merge. Preparatory tests yielded $c = 0.1$ as a suitable value to achieve this compromise. More detailed research is necessary to study the effect of a varying c or scale it to natural ice.

We refrain from any study of depth evolution of porosity, inclusion shape or distribution. In fact, the numerical microstructure evolution cannot be regarded as an evolution with depth like in natural firn and ice. However, the model can be used to study the behaviour of firn or bubbly ice, independent of the history that led to the particular microstructure. At all times during the simulation, we observe strain localisation controlled by air inclusions. This is even observed for small accumulated strains at low air contents (F05, Fig. 4). In addition, trial simulations showed that localisation also occurs at very different distributions of air inclusions at the same air fractions (see supplementary figure S1). There is no reason to expect that the strain localisation and elevated strain energies that drive dynamic recrystallisation that we observe for area-conservative pure shear would not occur during compaction.

Another approximation in the VPFFT approach is the treatment of the air phase. In the current model, air is treated as an ice Ih-symmetry crystal with equal basal, pyramidal and prismatic critical resolved shear stresses that are all 5000 times lower than for ice basal slip. This leaves the air phase slightly anisotropic. However, this assumption does not significantly affect the results since the effective contrast in slip resistance is significantly higher with a stress exponent of three (Eq. (1)). To further investigate any effects on the results, we compared our approach with an updated VPFFT code that avoids any crystallography in the air phase by imposing zero stiffness to air *unodes*, thus causing their stresses to vanish (Lebensohn et al., 2011; 2013). This was done by applying both our and the updated VPFFT approach to the initial setup of F20 for an increment of 1% vertical shortening to compute the instantaneous strain rate and stress distributions. The results are essentially the same for both setups (see supplementary figure S2) and show that the predictions of our simulations are not significantly affected by how we treat the air phase. Future simulations should include the optimized VPFFT approach imposing zero stiffness to air unodes.

Initial and final numerical grain sizes are larger than in natural firn, in particular with respect to the relatively high numerical strain rate. We chose to use initial grain sizes comparable to previous numerical simulations by Llorens et al. (2016a,b) and not to natural firn as other model assumptions would still hinder quantitative comparisons to natural samples. Adopting different grain boundary mobilities can significantly alter the resulting grain size. Therefore, we chose to use accepted literature values for grain boundary mobility as experimentally derived by Nasello et al. (2005) and used for previous numerical simulations by Roessiger et al. (2014), Llorens et al. (2016a,b) and Jansen et al. (2016). Although the use of lower mobilities would decrease the predicted grain sizes, the use of accepted literature values is more justified with respect to the scope of the study. Atomistic processes driving recrystallisation may be decelerated in nature due to the presence of impurities and pinning microparticles, which our simulation approach does not take into account. Any future comparison of simulations with natural ice may necessitate unexpectedly low or high values for material parameters such as an adapted

lower grain boundary mobility, to achieve a more realistic grain size. Investigating a more suitable numerical mobility remains part of future developments.

While the model scale affects the Elle recrystallisation processes and in turn grain sizes, the VPFFT approach is dimensionless and scale independent. The strain localisation bands and associated balance of recrystallisation driving forces is predicted by the VPFFT routine. This implies, that the main observations and interpretations drawn in this paper in relation to strain localisation remain valid independently of the numerical grain sizes.

5 Conclusions

We used polyphase numerical models of deformation and recrystallisation to investigate the occurrence of dynamic recrystallisation in an air-ice composite such as polar ice and firn. To our knowledge this provides the first full-field numerical simulation results on dynamic recrystallisation in polyphase crystalline aggregates in glaciology. ~~Our simulated microstructures resemble those from the EDML ice core site.~~ We show that strain and strain-rate localisation is to be expected during ice deformation, forming shear bands that accommodate significant amounts of strain. ~~Localisation is caused by the mechanical anisotropy of ice Ih that deforms by dislocation glide, and is intensified between air inclusions. We conclude that dynamic recrystallisation is occurring in very shallow levels of the ice sheet where it is related to strain localisation and stress concentrations between the air inclusions.~~ Dynamic recrystallisation can occur at relatively shallow levels of the ice sheet where it is related to strain localisation and stress concentrations between the air inclusions. This results in an increased heterogeneity in ice sheet deformation and more dynamic recrystallisation activity than previously assumed. In fact, strain localisation is probably not the exception, but the rule in ice sheets and glaciers. Wherever present, second phases such as air bubbles provide an effective mechanism for strain localisation in addition to mechanical anisotropy. Due to strain localisation, the rate of fabric change can be high locally, which is of special importance in firn, where bubbles are most abundant. The effects of localisation and heterogeneity in distribution of firn recrystallisation and deformation could be considered in future firn densification models. Furthermore, as the utilized VPFFT approach is dimensionless, future research could investigate the probably large range of scales at which strain localisation may occur in glaciers and ice sheets.

Acknowledgements

We are thankful for support and helpful discussions with the members of the Elle community. We thank Till Sachau, Sepp Kipfstuhl and Johannes Freitag for their input to improve the manuscript as well as the helpful comments by two anonymous reviewers. This study was funded by the DFG (SPP 1158) grant BO 1776/12-1. Furthermore, we acknowledge funding by the Helmholtz Junior Research group “The effect of deformation mechanisms for ice sheet dynamics” (VH-NG-802) and traveling funds for presenting and improving this study by the EPICA Descartes travel price, the ESF research networking

programme on the microdynamics of ice (MicroDICE) and the Helmholtz Graduate School for Polar and Marine Research (POLMAR).

References

Alley, R. B.: Texture of polar firn for remote sensing, Annals of Glaciology, 9, 1-4, 1987.

Alley, R. B., Gow, A. J., and Meese, D. A.: Mapping c-axis fabrics to study physical processes in ice, Journal of Glaciology, 41, 197-203, 1995.

Anderson, D. L., and Benson, C. S.: The densification and diagenesis of snow, in: Ice and Snow: Properties, Processes and Applications, MIT Press, 1963.

Arena, L., Nasello, O. B., and Levi, L.: Effect of bubbles on grain growth in ice, The Journal of Physical Chemistry B, 101, 6109-6112, 1997.

Azuma, N., and Higashi, A.: Formation processes of ice fabric pattern in ice sheets, Annals of Glaciology, 6, 130-134, 1985.

Azuma, N., Miyakoshi, T., Yokoyama, S., and Takata, M.: Impeding effect of air bubbles on normal grain growth of ice, Journal of Structural Geology, 42, 184-193, 2012.

Bachmann, F., Hielscher, R., and Schaeben, H.: Texture analysis with MTEX-free and open source software toolbox, Solid State Phenomena, 160, 63-68, 2010.

Becker, J. K., Bons, P. D., and Jessell, M. W.: A new front-tracking method to model anisotropic grain and phase boundary motion in rocks, Computers & Geosciences, 34, 201-212, 2008.

Blackford, J. R.: Sintering and microstructure of ice: a review, Journal of Physics D: Applied Physics, 40, R355, 2007.

Bons, P., Koehn, D., and Jessell, M.: Microdynamics Simulation, Volume 106 of Lecture Notes in Earth Sciences, Springer Berlin Heidelberg, 2008.

Bons, P. D., Jansen, D., Mundel, F., Bauer, C. C., Binder, T., Eisen, O., Jessell, M. W., Llorens, M.-G., Steinbach, F., Steinhage, D., and Weikusat, I.: Converging flow and anisotropy cause large-scale folding in Greenland's ice sheet, Nature Communications, 7, 2016.

Borthwick, V. E., Piazolo, S., Evans, L., Griera, A., and Bons, P. D.: What happens to deformed rocks after deformation? A refined model for recovery based on numerical simulations, Geological Society, London, Special Publications, 394, 215-234, 2014.

Brinckmann, S., Siegmund, T., and Huang, Y.: A dislocation density based strain gradient model, International Journal of Plasticity, 22, 1784-1797, 2006.

Budd, W., and Jacka, T.: A review of ice rheology for ice sheet modelling, Cold Regions Science and Technology, 16, 107-144, 1989.

Castelnau, O., Thorsteinsson, T., Kipfstuhl, J., Duval, P., and Canova, G.: Modelling fabric development along the GRIP ice core, central Greenland, Annals of Glaciology, 23, 194-201, 1996.

Colbeck, S.: Theory of metamorphism of dry snow, Journal of Geophysical Research: Oceans, 88, 5475-5482, 1983.

Davy, P., Hansen, A., Bonnet, E., and Zhang, S.-Z.: Localization and fault growth in layered brittle-ductile systems: Implications for deformations of the continental lithosphere, Journal of Geophysical Research: Solid Earth, 100, 6281-6294, 1995.

Cyprych, D., Brune, S., Piazolo, S., and Quinteros, J.: Strain localization in polycrystalline material with second phase particles: Numerical modeling with application to ice mixtures, Geochemistry, Geophysics, Geosystems, 2016.

De La Chapelle, S., Castelnau, O., Lipenkov, V., and Duval, P.: Dynamic recrystallization and texture development in ice as revealed by the study of deep ice cores in Antarctica and Greenland, Journal of Geophysical Research: Solid Earth, 103, 5091-5105, 1998.

Duval, P.: Creep and recrystallization of polycrystalline ice, Bulletin de Mineralogie, 102, 80-85, 1979.

Duval, P.: Grain growth and mechanical behaviour of polar ice, Annals of Glaciology, 6, 79-82, 1985.

Duval, P., and Castelnau, O.: Dynamic Recrystallization of Ice in Polar Ice Sheets, Journal de Physique IV, 05, C3-197-C193-205-C193, 1995.

Duval, P., Ashby, M. F., and Anderman, I.: Rate-controlling processes in the creep of polycrystalline ice, The Journal of Physical Chemistry, 87, 4066-4074, 1983.

Duval, P., Arnaud, L., Brissaud, O., Montagnat, M., and de La Chapelle, S.: Deformation and recrystallization processes of ice from polar ice sheets, Annals of Glaciology, 30, 83-87, 2000.

Faria, S. H., Freitag, J., and Kipfstuhl, S.: Polar ice structure and the integrity of ice-core paleoclimate records, Quaternary Science Reviews, 29, 338-351, 2010.

Faria, S. H., Weikusat, I., and Azuma, N.: The microstructure of polar ice. Part I: Highlights from ice core research, Journal of Structural Geology, 61, 2-20, 2014a.

Faria, S. H., Weikusat, I., and Azuma, N.: The microstructure of polar ice. Part II: State of the art, Journal of Structural Geology, 61, 21-49, 2014b.

Fischer, H., Behrens, M., Bock, M., Richter, U., Schmitt, J., Loulergue, L., Chappellaz, J., Spahni, R., Blunier, T., Leuenberger, M., and Stocker, T. F.: Changing boreal methane sources and constant biomass burning during the last termination, Nature, 452, 864-867, 2008.

Fliervoet, T. F., White, S. H., and Drury, M. R.: Evidence for dominant grain-boundary sliding deformation in greenschist- and amphibolite-grade polymineralic ultramylonites from the Redbank Deformed Zone, Central Australia, Journal of Structural Geology, 19, 1495-1520, 1997.

Freitag, J., Kipfstuhl, S., and Faria, S. H.: The connectivity of crystallite agglomerates in low-density firn at Kohnen station, Dronning Maud Land, Antarctica, Annals of Glaciology, 49, 114-120, 2008.

Gao, X., and Jacka, T.H.: The approach to similar tertiary creep rates for Antarctic core ice and laboratory prepared ice, Le Journal de Physique Colloques, 48, C1-289-C281-296, 1987.

Glen, J.: The flow law of ice: A discussion of the assumptions made in glacier theory, their experimental foundations and consequences, IASH Publ, 47, 171-183, 1958.

Goldsby, D. L.: Superplastic Flow of Ice Relevant to Glacier and Ice-Sheet Mechanics, Glacier Science and Environmental Change, 308-314, 2006.

Gow, A. J.: On the rates of growth of grains and crystals in south polar firn, Journal of Glaciology, 8, 241-252, 1969.

Griera, A., Bons, P. D., Jessell, M. W., Lebensohn, R. A., Evans, L., and Gomez-Rivas, E.: Strain localization and porphyroclast rotation, Geology, 39, 275-278, 2011.

Griera, A., Llorens, M.-G., Gomez-Rivas, E., Bons, P. D., Jessell, M. W., Evans, L. A., and Lebensohn, R.: Numerical modelling of porphyroclast and porphyroblast rotation in anisotropic rocks, Tectonophysics, 587, 4-29, 2013.

Herron, M. M., and Langway Jr, C. C.: Firn densification: an empirical model, Journal of Glaciology, 25, 373-385, 1980.

Hirth, G., and Tullis, J.: Dislocation creep regimes in quartz aggregates, Journal of Structural Geology, 14, 145-159, 1992.

Humphreys, F. J., and Hatherly, M.: Recrystallization and related annealing phenomena, Elsevier, 2004.

Jacka, T. H., and Li, J.: The steady-state crystal size of deforming ice, Annals of Glaciology, 20, 13-18, 1994.

Jansen, D., Llorens, M. G., Westhoff, J., Steinbach, F., Kipfstuhl, S., Bons, P. D., Griera, A., and Weikusat, I.: Small-scale disturbances in the stratigraphy of the NEEM ice core: observations and numerical model simulations, The Cryosphere, 10, 359-370, 2016.

Jessell, M., Bons, P., Evans, L., Barr, T., and Stüwe, K.: Elle: the numerical simulation of metamorphic and deformation microstructures, Computers & Geosciences, 27, 17-30, 2001.

Jessell, M. W., Bons, P. D., Griera, A., Evans, L. A., and Wilson, C. J. L.: A tale of two viscosities, Journal of Structural Geology, 31, 719-736, 2009.

Ketcham, W. M., and Hobbs, P. V.: An experimental determination of the surface energies of ice, Philosophical Magazine, 19, 1161-1173, 1969.

Kipfstuhl, S., Hamann, I., Lambrecht, A., Freitag, J., Faria, S. H., Grigoriev, D., and Azuma, N.: Microstructure mapping: a new method for imaging deformation-induced microstructural features of ice on the grain scale, Journal of glaciology, 52, 398-406, 2006.

Kipfstuhl, S., Faria, S. H., Azuma, N., Freitag, J., Hamann, I., Kaufmann, P., Miller, H., Weiler, K., and Wilhelms, F.: Evidence of dynamic recrystallization in polar firn, Journal of Geophysical Research: Solid Earth (1978-2012), 114, 2009.

Krischke, A., Oechsner, U., and Kipfstuhl, S.: Rapid Microstructure Analysis of Polar Ice Cores, Optik & Photonik, 10, 32-35, 2015.

Lebensohn, R. A.: N-site modeling of a 3D viscoplastic polycrystal using Fast Fourier Transform, Acta Materialia, 49, 2723-2737, 2001.

Lebensohn, R. A., Montagnat, M., Mansuy, P., Duval, P., Meysonnier, J., and Philip, A.: Modeling viscoplastic behavior and heterogeneous intracrystalline deformation of columnar ice polycrystals, Acta Materialia, 57, 1405-1415, 2009.

Lebensohn, R., Idiart, M., Castañeda, P. P., and Vincent, P.-G.: Dilatational viscoplasticity of polycrystalline solids with intergranular cavities, Philosophical Magazine, 91, 3038-3067, 2011.

Lebensohn, R. A., Escobedo, J. P., Cerreta, E. K., Dennis-Koller, D., Bronkhorst, C. A., and Bingert, J. F.: Modeling void growth in polycrystalline materials, Acta Materialia, 61, 6918-6932, 2013.

Llorens, M.-G., Bons, P. D., Griera, A., and Gomez-Rivas, E.: When do folds unfold during progressive shear? Geology, 41, 563-566, 2013a.

Llorens, M.-G., Bons, P. D., Griera, A., Gomez-Rivas, E., and Evans, L. A.: Single layer folding in simple shear, Journal of Structural Geology, 50, 209-220, 2013b.

Llorens, M.-G., Griera, A., Bons, P. D., Roessiger, J., Lebensohn, R., Evans, L., and Weikusat, I.: Dynamic recrystallisation of ice aggregates during co-axial viscoplastic deformation: a numerical approach, Journal of Glaciology, FirstView, 1-19, 2016a.

Llorens, M.-G., Griera, A., Bons, P. D., Lebensohn, R., Evans, L., Jansen, D. and Weikusat, I.: Full-field prediction of ice dynamic recrystallisation under simple shear conditions, Earth and Planetary Science Letters, 2016b, in press, DOI: 10.1016/j.epsl.2016.06.045

Luethi, D., Le Floch, M., Bereiter, B., Blunier, T., Barnola, J.-M., Siegenthaler, U., Raynaud, D., Jouzel, J., Fischer, H., Kawamura, K., and Stocker, T. F.: High-resolution carbon dioxide concentration record 650,000-800,000 years before present, Nature, 453, 379-382, 2008.

Maeno, N., and Ebinuma, T.: Pressure sintering of ice and its implication to the densification of snow at polar glaciers and ice sheets, The Journal of Physical Chemistry, 87, 4103-4110, 1983.

Mainprice, D., Hielscher, R., and Schaeben, H.: Calculating anisotropic physical properties from texture data using the MTEX open-source package, Geological Society, London, Special Publications, 360, 175-192, 2011.

~~Montagnat, M., Blackford, J. R., Piazolo, S., Arnaud, L., and Lebensohn, R. A.: Measurements and full-field predictions of deformation heterogeneities in ice, Earth and Planetary Science Letters, 305, 153-160, 2011.~~

Montagnat, M., Castelnau, O., Bons, P. D., Faria, S. H., Gagliardini, O., Gillet-Chaulet, F., Grennerat, F., Griera, A., Lebensohn, R. A., Moulinec, H., Roessiger, J., and Suquet, P.: Multiscale modeling of ice deformation behavior, Journal of Structural Geology, 61, 78-108, 2014.

Nasello, O. B., Prinzio, C. L. D., and Guzmán, P. G.: Temperature dependence of “pure” ice grain boundary mobility, Acta Materialia, 53, 4863-4869, 2005.

Oerter, H., Druecker, C., Kipfstuhl, S., and Wilhelms, F.: Kohnen station-the drilling camp for the EPICA deep ice core in Dronning Maud Land, 2009.

Passchier, C. W., and Trouw, R. A. J.: Microtectonics, Springer, 2005.

Petrenko, V. F., and Whitworth, R. W.: Physics of ice, Clarendon Press, 1999.

Piazolo, S., Jessell, M. W., Bons, P. D., Evans, L., and Becker, J. K.: Numerical simulations of microstructures using the Elle platform: a modern research and teaching tool, Journal of the Geological Society of India, 75, 110-127, 2010.

Riche, F., Montagnat, M., and Schneebeli, M.: Evolution of crystal orientation in snow during temperature gradient metamorphism, Journal of Glaciology, 59, 47-55, 2013.

Rignot, E., Mouginot, J., and Scheuchl, B.: Ice flow of the Antarctic ice sheet, Science, 333, 1427-1430, 2011.

Roessiger, J., Bons, P. D., Griera, A., Jessell, M. W., Evans, L., Montagnat, M., Kipfstuhl, S., Faria, S. H., and Weikusat, I.: Competition between grain growth and grain-size reduction in polar ice, Journal of Glaciology, 57, 942-948, 2011.

Roessiger, J., Bons, P. D., and Faria, S. H.: Influence of bubbles on grain growth in ice, Journal of Structural Geology, 61, 123-132, 2014.

Ruth, U., Barnola, J. M., Beer, J., Bigler, M., Blunier, T., Castellano, E., Fischer, H., Fundel, F., Huybrechts, P., Kaufmann, P., Kipfstuhl, S., Lambrecht, A., Morganti, A., Oerter, H., Parrenin, F., Rybak, O., Severi, M., Udisti, R., Wilhelms, F., and Wolff, E.: "EDML1": a chronology for the EPICA deep ice core from Dronning Maud Land, Antarctica, over the last 150 000 years, Clim. Past, 3, 475-484, 2007

Schulson, E. M., and Duval, P.: Creep and fracture of ice, Cambridge University Press Cambridge, 2009.

Schwander, J., and Stauffer, B.: Age difference between polar ice and the air trapped in its bubbles, Nature, 311, 45-47, 1984.

Shoji, H., and Higashi, A.: A deformation mechanism map of ice, Journal of Glaciology, 21, 419-427, 1978.

Sornette, A., Davy, P., and Sornette, D.: Fault growth in brittle-ductile experiments and the mechanics of continental collisions, Journal of Geophysical Research: Solid Earth, 98, 12111-12139, 1993.

Stauffer, B., Schwander, J., and Oeschger, H.: Enclosure of air during metamorphosis of dry firn to ice, Annals of Glaciology, 6, 108-112, 1985.

Steinemann, S.: Flow and recrystallization of ice, IASH Publ, 39, 449-462, 1954.

Stephenson, P. J.: Some considerations of snow metamorphism in the Antarctic ice sheet in the light of ice crystal studies, Physics of Snow and Ice, 1, 725-740, 1967.

Theile, T., Löwe, H., Theile, T. C., and Schneebeli, M.: Simulating creep of snow based on microstructure and the anisotropic deformation of ice, Acta Materialia, 59, 7104-7113, 2011.

Treverrow, A., Budd, W. F., Jacka, T. H., and Warner, R. C.: The tertiary creep of polycrystalline ice: experimental evidence for stress-dependent levels of strain-rate enhancement, Journal of Glaciology, 58, 301-314, 2012.

Urai, J. L., Means, W. D., and Lister, G. S.: Dynamic recrystallization of minerals, in: Mineral and rock deformation: laboratory studies, American Geophysical Union Washington, DC, 161-199, 1986.

Weikusat, I., Kipfstuhl, S., Faria, S. H., Azuma, N., and Miyamoto, A.: Subgrain boundaries and related microstructural features in EDML (Antarctica) deep ice core, Journal of Glaciology, 55, 461-472, 2009.

Weikusat, I., de Winter, D., Pennock, G., Hayles, M., Schneijdenberg, C., and Drury, M.: Cryogenic EBSD on ice: preserving a stable surface in a low pressure SEM, Journal of microscopy, 242, 295-310, 2011a.

Weikusat, I., Miyamoto, A., Faria, S. H., Kipfstuhl, S., Azuma, N., and Hondoh, T.: Subgrain boundaries in Antarctic ice quantified by X-ray Laue diffraction, Journal of Glaciology, 57, 111-120, 2011b.

White, S.: Geological significance of recovery and recrystallization processes in quartz, Tectonophysics, 39, 143-170, 1977.

Table 1: Input properties for the simulations F00, F05 and F20. Remaining input properties according to Llorens et al. (2016, Table 1). A more detailed description of the parameters is provided in sections 2.4 and 2.6 and Llorens et al. (2016a,b).

Symbol	Explanation	Input value
	Minimum *bnode* separation	2.5 x 10^{-4} m
	Maximum *bnode* separation	5.5 x 10^{-4} m
	Time step per simulation step	10^{8} s
	Ratio of time step between VPFFT and recrystallisation codes	20
	Number of recrystallisation subloops per one step of VPFFT within one simulation step	20
	Incremental strain per simulation step	0.01
$\tau_{basal} / \tau_{non\text{-}basal}$	Ice Ih: Ratio non-basal / basal glide resistance	20
$\tau_{basal} / \tau_{s\text{-}air}$	Air: Ratio ice Ih basal resistance/air flow stress	5000
$M_{ice\text{-}ice}$	Intrinsic mobility of ice-ice boundaries (Nasello et al., 2005)	0.023 m^4 J^{-1} s^{-1}
$M_{ice\text{-}air}$	Intrinsic mobility of ice-air boundaries (Roessiger et al., 2014)	0.0023 m^4 J^{-1} s^{-1}
$\gamma_{ice\text{-}ice}$	Ice-ice interface surface energy (Ketcham and Hobbs, 1969)	0.065 J m^{-2}
$\gamma_{ice\text{-}air}$	Ice-air interface surface energy (Roessiger et al., 2014)	0.52 J m^{-2}
	Resulting dihedral angle at ice air triple junctions (Roessiger et al., 2014)	173 °
α_{hagb}	Critical misorientation: ice high angle boundary (Weikusat et al., 2010; 2011)	5 °
c	Area energy or compressibility factor (10 times the value of Roessiger et al., 2014)	0.1

Table 2: Overview on numerical simulations using crystal visco-plasticity and dynamic recrystallisation (DRX) and only normal grain growth (NGG) simulations. NGG simulations used the same initial microstructures than DRX simulations.

	Area fraction of air	**Initial number of ice grains**	**Final number of ice grains DRX (*NGG*)**	**Initial mean ice grain area and (*standard deviation*)**	**DRX: Final mean ice grain area and (*standard deviation*)**	**NGG: Final mean ice grain area and (*standard deviation*)**	**Final and (*initial*) first eigenvalue of CPO**
F00	0 %	3267	1631 (*1093*)	6.12 mm² (*3.50 mm²*)	12.17 mm² (*12.26 mm²*)	18.30 mm² (*13.25 mm²*)	0.~~8032~~7603 (*0.~~6692~~3393*)
F05	5 %	3128	1994 (*1155*)	6.07 mm² (*3.43 mm²*)	9.44 mm² (*10.87 mm²*)	16.43 mm² (*12.34 mm²*)	0.~~7613~~6975 (*0.~~6663~~3390*)
F20	20 %	2654	1891 (*1265*)	5.96 mm² (*3.33 mm²*)	8.30 mm² (*9.80 mm²*)	12.53 mm² (*10.52 mm²*)	0.~~6933~~5665 (*0.~~6649~~3468*)

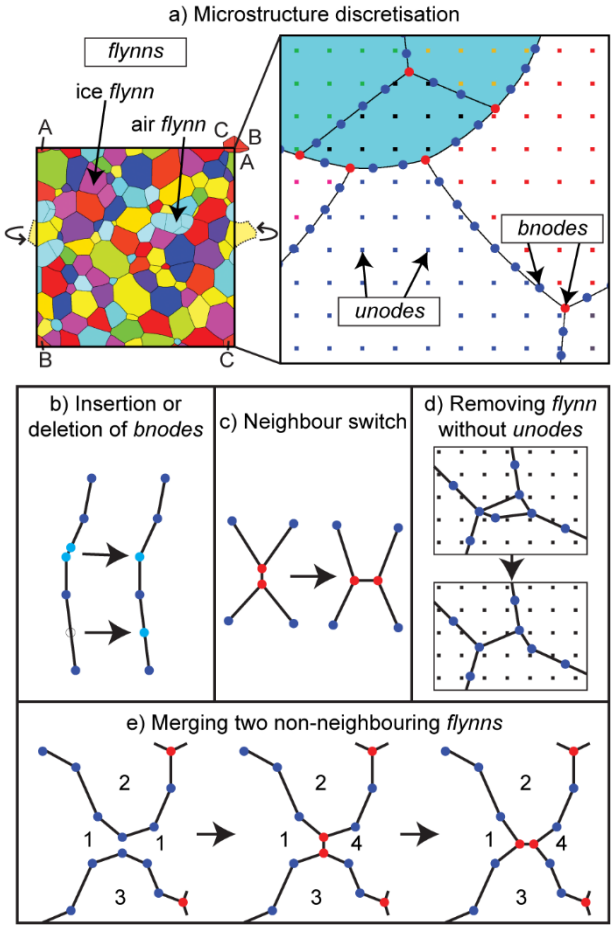

Figure 1: Microstructure discretisation in Elle. (a) A contiguous set of polygons (flynns) is composed of boundary nodes (bnodes) and has periodic boundaries. An additional grid of unconnected nodes (unodes) is superimposed on flynns and bnodes to store intracrystalline properties, state variables and track deformation. (b-e) Topological checks performed to keeping topological restrictions in Elle. Checks (b), (c) and (e) are based on minimum and maximum bnode separations. Check (d) removes extremely small flynns that contain no undoes or have areas smaller than the area enclosed by four neighbouring unodes by merging them to a neighbour of the same phase.

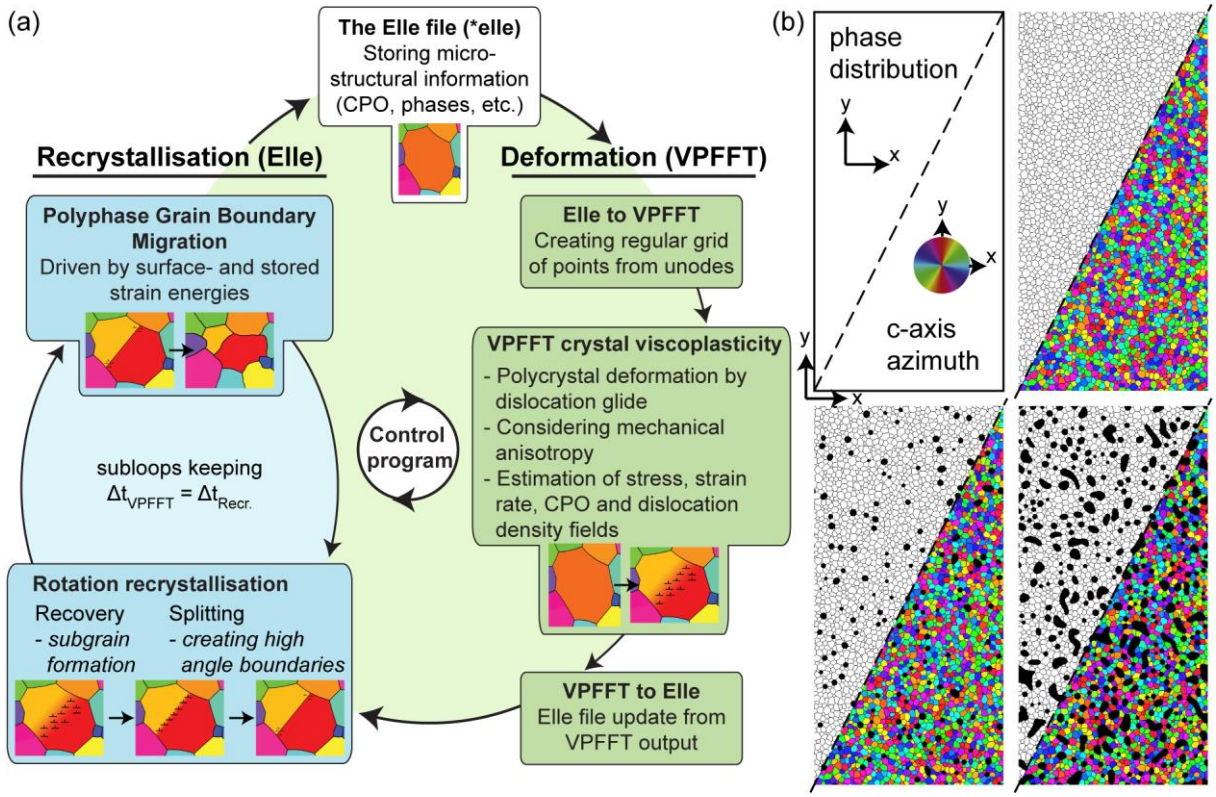

Figure 2: (a) Multi-process modelling by operator splitting is achieved by successively running individual process modules. One step of deformation by VPFFT code is followed by five subloops (with shorter time steps) of recrystallisation, each comprising four steps of recovery and grain-boundary migration, to keep a constant time step for all combined processes. (b) Initial 10x20 cm microstructures with foam textures containing 0 %, 5 % and 20 % of air and with an initially random crystallographic fabric. Upper left half shows grain boundary network, lower right the lattice orientations.

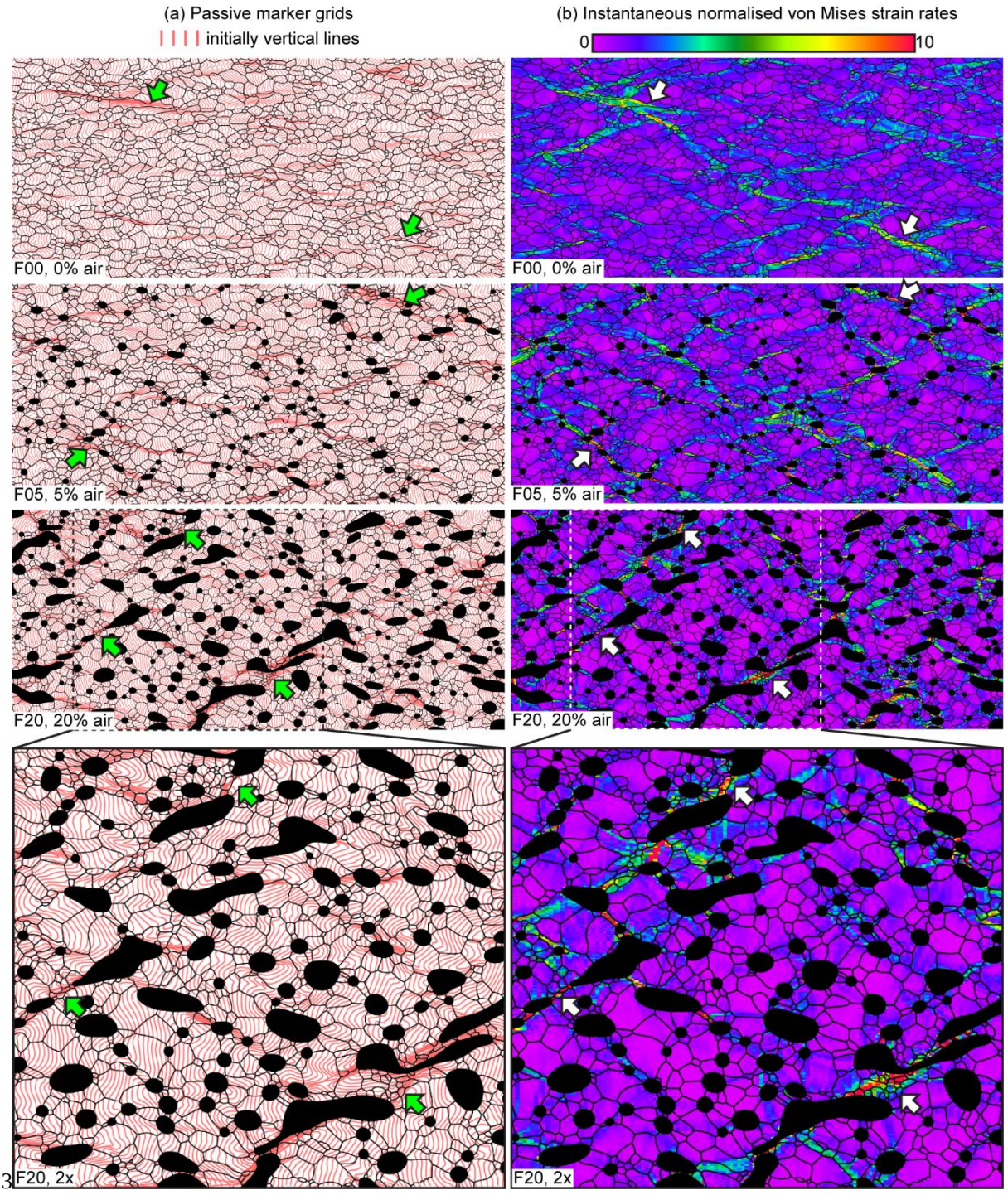

Figure 3: Overview of modelling results at last time step at 53 % vertical shortening under pure shear conditions. (a) Grain boundary network superimposed on passive marker grid of initially vertical parallel lines to show the finite strain distribution. (b) The same microstructures superimposed on the map of instantaneous strain rates expressed as von Mises strain rates normalized to the bulk value. Arrows in both images indicate zones of marked strain localisation. Air inclusions are displayed in black.

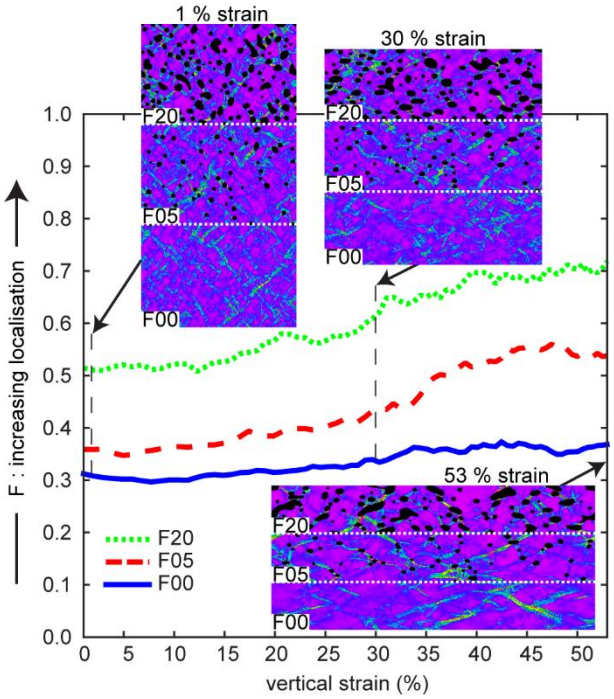

Figure 4: Evolution of localisation factors (F) with strain quantifying strain localisation in the microstructures for all simulations. A factor of 0 represents homogeneous deformation, the factor increases towards one with increased strain-rate heterogeneity and localisation. The normalized von Mises strain rate maps at 1 %, 30 % and 53 % vertical strain are shown for reference. The maps are subdivided to show results of simulation F20 in the upper third, of F05 in the middle and F00 in the lower third part of the model box. They illustrate strain localisation at different stages of the simulation.

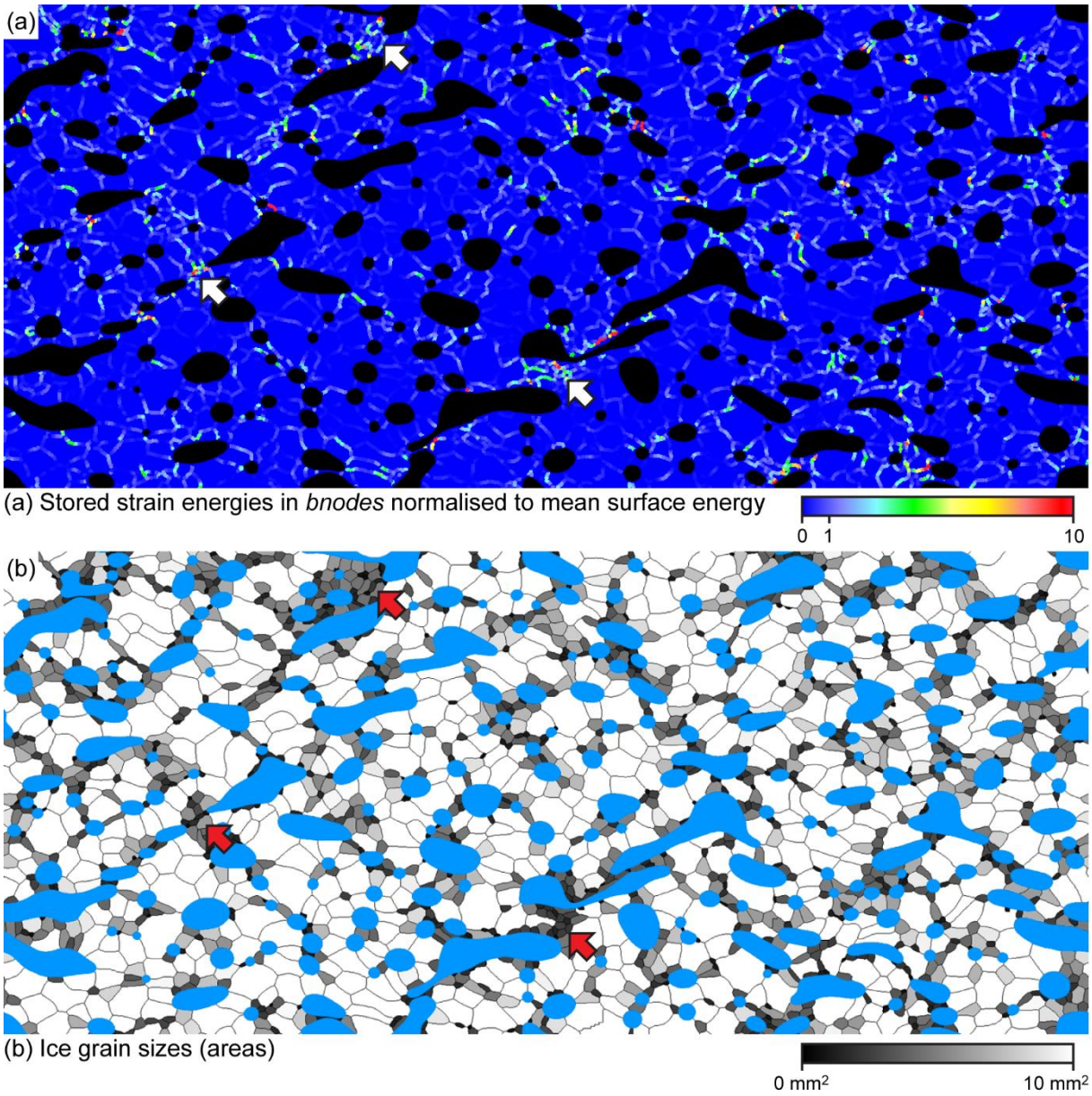

Figure 5: Details of results of simulation F20 at 53% vertical shortening: (a) Boundary nodes colour coded according to the proportion of strain-induced boundary migration. Air inclusions are plotted in black since they do not contribute to strain induced boundary migration. (b) Microstructure colour-coded according to the areas of ice grains, with air inclusions displayed in blue. Smallest grains appear grey to black. Arrows in both images indicate zones of marked strain localisation.

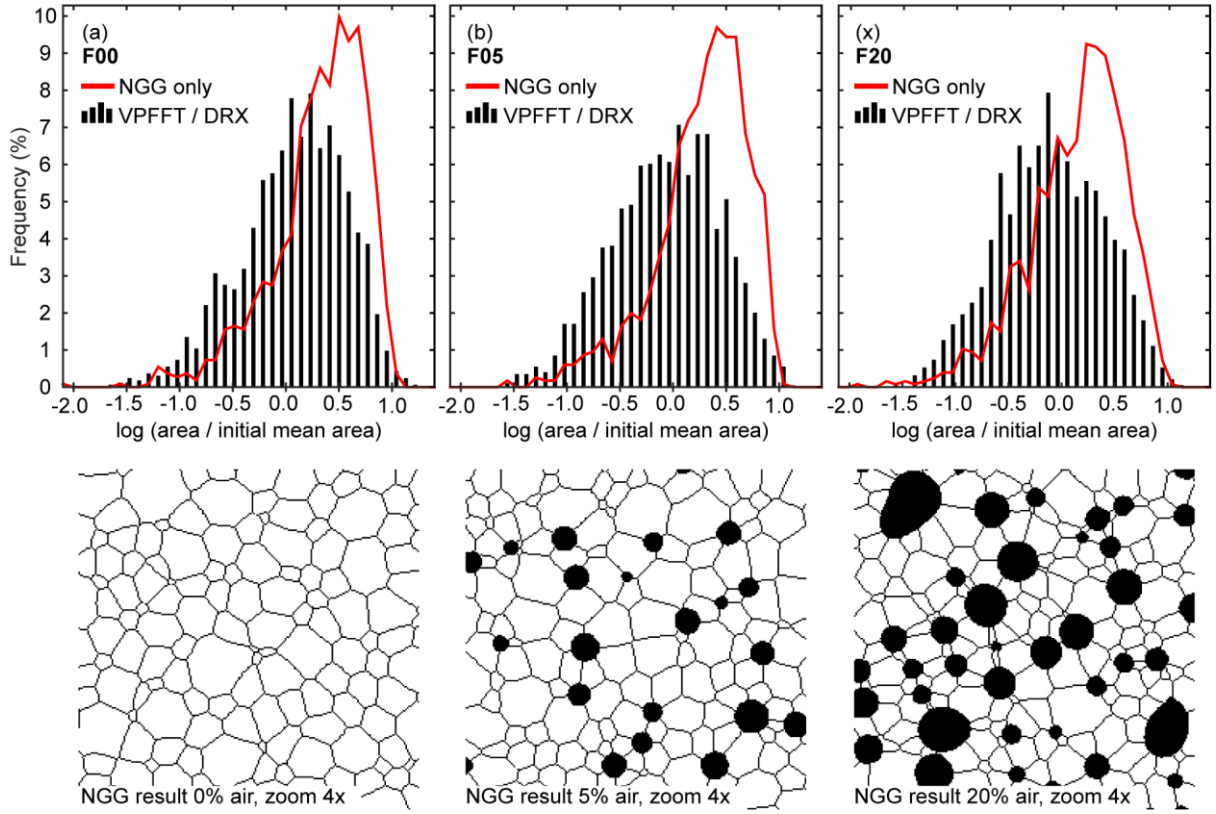

Figure 6: Comparison of ice grain area histograms of the last simulation step of simulations (a) F00, (b) F05 and (c) F20. Normal grain growth (NGG) simulations using F00, F05 and F20 input models are displayed with the respective deformation and dynamic recrystallisation (VPFFT / DRX) simulation results. Areas were normalized to initial mean values that plot at a value of 0.0 on x-axis. For reference, a fourfold zoom in the resulting microstructures from NGG simulations is displayed below the histograms.

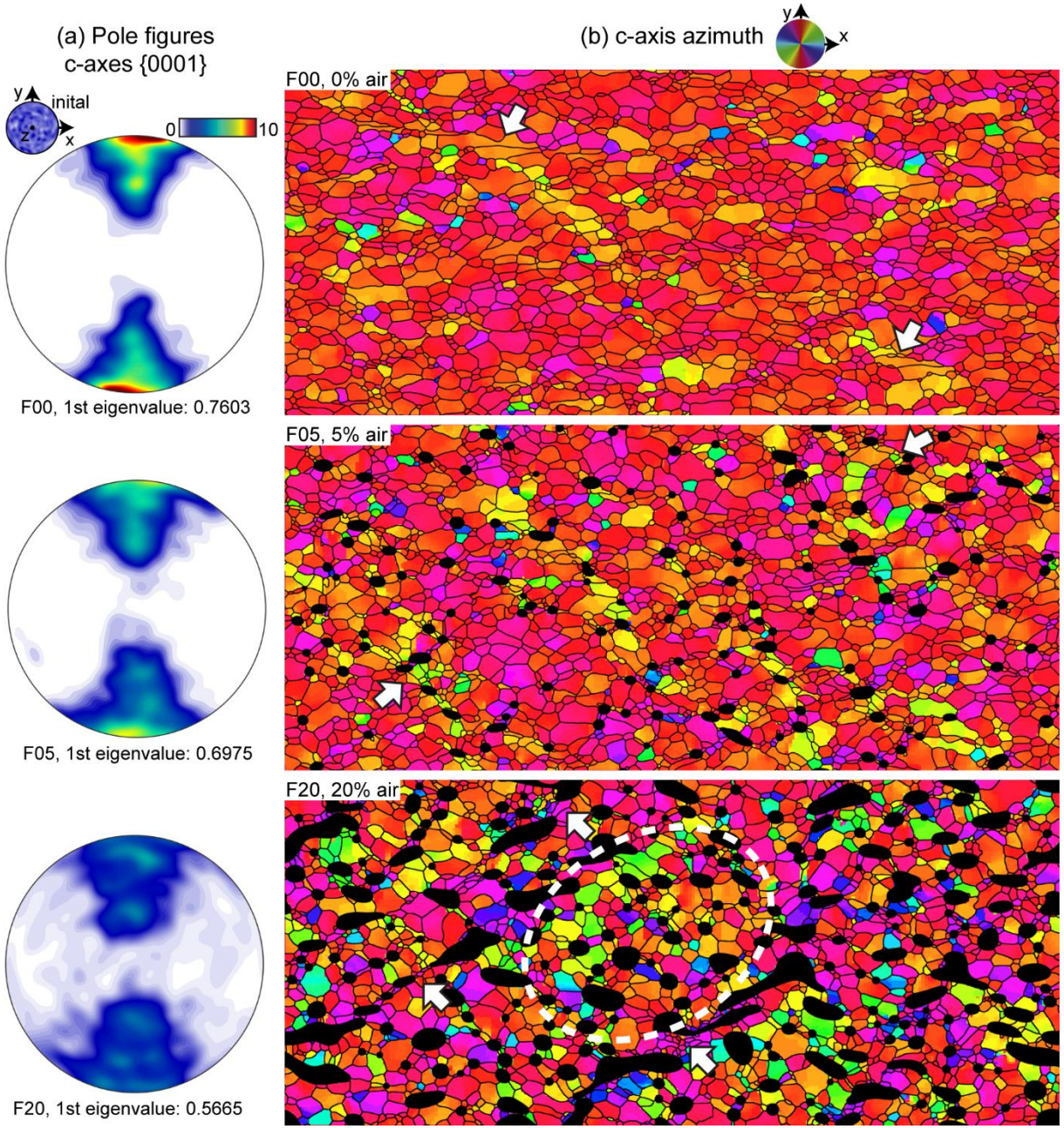

Figure 7: Overview of c-axis orientations at 53 % vertical shortening for all simulations. (a) Pole figures with the projection plane parallel to the *x*-*y* plane of the 2D model. (b) Maps of c-axis azimuth distributions. Air inclusions are shown in black. White arrows in both images indicate zones of marked strain localisation. Dotted white line indicates zone of low strain where more random crystallographic orientations are preserved.

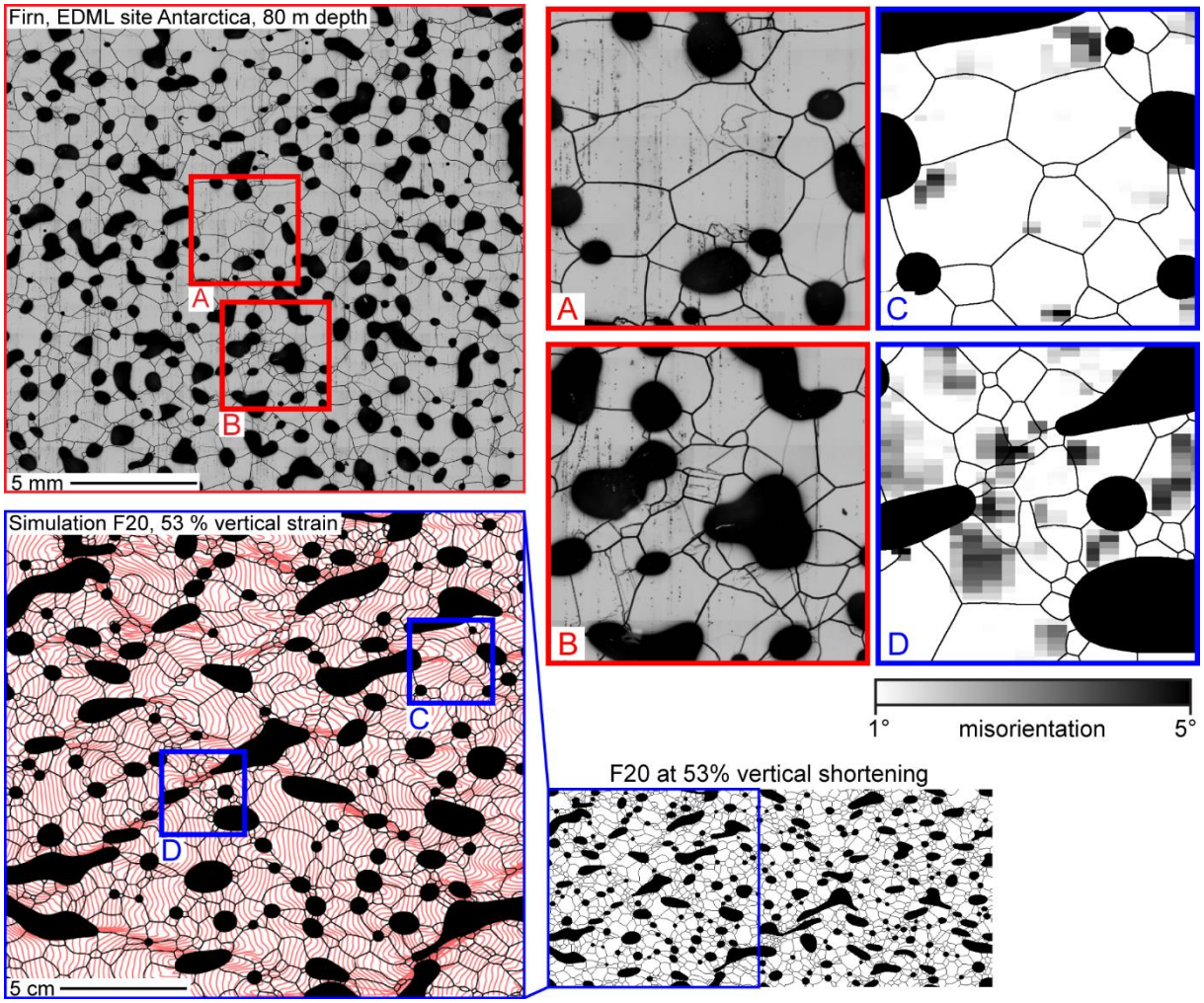

Figure 8: Comparison of simulation results of F20 at 53% vertical shortening with firn microstructure mapping images from the EDML ice core site at 80 m depth (courtesy of Sepp Kipfstuhl). The detail areas A-D illustrate different microstructures occurring in relation to strain localisation. Grain boundaries stand out as black lines and subgrain boundaries are visible as fainter grey lines. Vertical stripes appearing in the overview image are related to the sample polishing technique and not reflecting any microstructural property. Greyscales C and D indicate local average misorientations as stored in *unodes* and therefore appear blurred due to the strong magnification. Note however, that strain paths of the natural microstructure (compaction) and the simulation (pure shear) are not identical and the comparison is restricted to the microstructural similarities and inferred localisation and recrystallisation processes.